Tran-SET

Transportation Consortium of South-Central States

Solving Emerging Transportation Resiliency, Sustainability, and Economic Challenges through the Use of Innovative Materials and Construction Methods: From Research to Implementation

A Comprehensive Reliability-Based Framework for Corrosion Damage Monitoring and Repair Design of Reinforced Concrete Structures

Project No. 17STLSU03

Lead University: Texas A&M University

Collaborative Universities: Louisiana State University, University of New Mexico

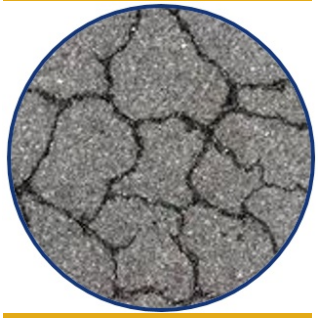

Enhancing Durability and Service Life of Infrastructure

Final Report

December 2018

Disclaimer

The contents of this report reflect the views of the authors, who are responsible for the facts and the accuracy of the information presented herein. This document is disseminated in the interest of information exchange. The report is funded, partially or entirely, by a grant from the U.S. Department of Transportation's University Transportation Centers Program. However, the U.S. Government assumes no liability for the contents or use thereof.

Acknowledgments

The authors would like to acknowledge the laboratory support and field results by CINVESTAV, Merida and the technical expertise from Pedro Castro and Mercedes Balankan. The authors would also like to acknowledge Luke Nyakity (Texas A&M University at Galveston), Doeun Choe (Prairie View A&M University), and Ivan Karajan (Texas A&M University).

TECHNICAL DOCUMENTATION PAGE

1. Project No.	2. Government Accession No.	3. Recipient's Catalog No.
17STLSU03		

4. Title and Subtitle	5. Report Date
A Comprehensive Reliability-Based Framework for Corrosion Damage Monitoring and Repair Design of Reinforced Concrete Structures	Dec. 2018 **6. Performing Organization Code**
7. Author(s) PI: Homero Castaneda https://orcid.org/0000-0002-9252-7744 Co-PI: Aydin I. Karsilayan https://orcid.org/000-0001-8694-8836 Co-PI: Ayman M. Okeil https://orcid.org/0000-0001-9685-9458 Co-PI: Mahmoud Reda Taha htpps://orcid.org/0000-0002-3707-9336	**8. Performing Organization Report No.**
9. Performing Organization Name and Address Transportation Consortium of South-Central States (Tran-SET) University Transportation Center for Region 6 3319 Patrick F. Taylor Hall, Louisiana State University, Baton Rouge, LA 70803	**10. Work Unit No. (TRAIS)** **11. Contract or Grant No.** 69A3551747106
12. Sponsoring Agency Name and Address United States of America Department of Transportation Research and Innovative Technology Administration	**13. Type of Report and Period Covered** Final Research Report May 2017 – May 2018 **14. Sponsoring Agency Code**

15. Supplementary Notes

Report uploaded and accessible at: Tran-SET's website (http://transet.lsu.edu/)

16. Abstract

In this work, we developed a comprehensive framework for corrosion management of reinforced concrete (RC) structures. This framework includes critical steps of an effective approach to quantify the damage evolution as well as providing the timeframe for effective maintenance/repair strategies for corrosion assessment in RC structures. The framework included several activities including the use of indirect and direct inspection tools, theoretical development for damage prediction, experimental measurements and theoretical development of repair time based on reliability. The uniqueness of the framework is the integration of deterministic modeling of corrosion damage evolution by using mechanistic analysis with statistical modeling on corrosion of RC structures by using measurements from the field (or natural environment) and experimental testing (in the laboratory). The framework includes a simple algorithm that relies in each development and task generated from this work to monitor and estimate the status of the reinforced concrete structures and the most suitable strategy to extend the life of the system while maximizing the reliability.

17. Key Words	18. Distribution Statement
Corrosion Monitoring, Reliability, Concrete Repairing	No restrictions.

19. Security Classif. (of this report)	20. Security Classif. (of this page)	21. No. of Pages	22. Price
Unclassified	Unclassified	50	

Form DOT F 1700.7 (8-72) **Reproduction of completed page authorized.**

SI* (MODERN METRIC) CONVERSION FACTORS

APPROXIMATE CONVERSIONS TO SI UNITS

Symbol	When You Know	Multiply By	To Find	Symbol
		LENGTH		
in	inches	25.4	millimeters	mm
ft	feet	0.305	meters	m
yd	yards	0.914	meters	m
mi	miles	1.61	kilometers	km
		AREA		
in^2	square inches	645.2	square millimeters	mm^2
ft^2	square feet	0.093	square meters	m^2
yd^2	square yard	0.836	square meters	m^2
ac	acres	0.405	hectares	ha
mi^2	square miles	2.59	square kilometers	km^2
		VOLUME		
fl oz	fluid ounces	29.57	milliliters	mL
gal	gallons	3.785	liters	L
ft^3	cubic feet	0.028	cubic meters	m^3
yd^3	cubic yards	0.765	cubic meters	m^3
		NOTE: volumes greater than 1000 L shall be shown in m^3		
		MASS		
oz	ounces	28.35	grams	g
lb	pounds	0.454	kilograms	kg
T	short tons (2000 lb)	0.907	megagrams (or "metric ton")	Mg (or "t")
		TEMPERATURE (exact degrees)		
^oF	Fahrenheit	5 (F-32)/9 or (F-32)/1.8	Celsius	^oC
		ILLUMINATION		
fc	foot-candles	10.76	lux	lx
fl	foot-Lamberts	3.426	candela/m^2	cd/m^2
		FORCE and PRESSURE or STRESS		
lbf	poundforce	4.45	newtons	N
lbf/in^2	poundforce per square inch	6.89	kilopascals	kPa

APPROXIMATE CONVERSIONS FROM SI UNITS

Symbol	When You Know	Multiply By	To Find	Symbol
		LENGTH		
mm	millimeters	0.039	inches	in
m	meters	3.28	feet	ft
m	meters	1.09	yards	yd
km	kilometers	0.621	miles	mi
		AREA		
mm^2	square millimeters	0.0016	square inches	in^2
m^2	square meters	10.764	square feet	ft^2
m^2	square meters	1.195	square yards	yd^2
ha	hectares	2.47	acres	ac
km^2	square kilometers	0.386	square miles	mi^2
		VOLUME		
mL	milliliters	0.034	fluid ounces	fl oz
L	liters	0.264	gallons	gal
m^3	cubic meters	35.314	cubic feet	ft^3
m^3	cubic meters	1.307	cubic yards	yd^3
		MASS		
g	grams	0.035	ounces	oz
kg	kilograms	2.202	pounds	lb
Mg (or "t")	megagrams (or "metric ton")	1.103	short tons (2000 lb)	T
		TEMPERATURE (exact degrees)		
^oC	Celsius	1.8C+32	Fahrenheit	^oF
		ILLUMINATION		
lx	lux	0.0929	foot-candles	fc
cd/m^2	candela/m^2	0.2919	foot-Lamberts	fl
		FORCE and PRESSURE or STRESS		
N	newtons	0.225	poundforce	lbf
kPa	kilopascals	0.145	poundforce per square inch	lbf/in^2

TABLE OF CONTENTS

LIST OF FIGURES

LIST OF TABLES

ACRONYMS, ABBREVIATIONS, AND SYMBOLS

AC	Alternating Current
AIC	Akaike Information Criterion
BIC	Bayesian Information Criterion
CDF	Cumulative Distribution Function
COV	Coefficient of Variation
DC	Direct Current
DOT	Department of Transportation
EIS	Electrochemical Impedance Spectroscopy
FORM	First Order Reliability Method
i_{corr}	Corrosion Current Density
LRFD	Load and Resistance Factor Design
MCS	Monte Carlo Simulations
NACE	National Corrosion Association Engineers
RC	Reinforced Concrete
TAMU	Texas A&M University
w/c	Water to Cement Ratio

EXECUTIVE SUMMARY

A comprehensive framework was developed in this study by combining the experimental characterization, electrochemical fundamentals, and mathematical modeling based on two probabilistic modeling approaches. The experimental characterization included various reinforced concrete (RC) samples exposed to off-shore conditions at different locations close to the Gulf of Mexico. Sample preparation included different concrete properties and exposure times. There were two different sets of samples: the first set was initiated for several months (more than 60 months before the initiation of this work), and the second set when this project started. While the first batch included i_{corr} (corrosion current by a polarization technique) measurements, the second used an electrochemical method (electrochemical impedance spectroscopy) to characterize and measure the state of the rebar in the exposed conditions. These two experimental sets provide information about the corrosion kinetics of the rebar in concrete structures and data generation for validation of one of the probabilistic models. The longer exposure samples guided the computational/mechanistic part of the framework to produce an evidence-based probabilistic corrosion initiation model for RC structures, which predicts the corrosion initiation time and determines the existing variance, considering different materials (water-cement ratio, days of curing) and environmental conditions (offshore distance) of the RC samples. A Bayesian methodology was the core of the model for the parameter estimation, updating, and model selection procedures. The Bayesian type probabilistic model was used to estimate the probability of corrosion initiation under the given time and concrete material conditions. The sensitivity analyses identified the most influencing parameters for improving the reliability, which contributes to decision-making, thereby improving the corrosion control method. A second model using a semi-empirical degradation function was included to establish a reliability-based framework for service life prediction, using the uncertainties characteristically recognized in the parameters identified and quantified from an established corrosion detection process. Reliability algorithms, such as the First Order Reliability Model (FORM) procedures, were used for this second approach. Using the reliability-calibrated design factors, our aim was to address the effects of the various factors within particular corrosion conditions, thereby joining the service life prediction model to the design of repair and strengthening work, as well as load rating, of RC structures.

By following the proposed computational framework, our Bayesian-based model can be updated, improved, and modified using datasets that become available in the future. In the second model, the FORM is used to analyze the structural reliability problem. Both models show how this framework can be used to help infrastructure owners make maintenance and repair decisions to achieve their goals (e.g., extend service life). The models cited in the proposed methodology for the reliability framework achieve one of the main goals of this work: to estimate the structural degradation of RC structures and infrastructures based on degradation mechanisms and monitoring tools for corrosion. Finally, the experimental data obtained by electrochemical methods helped us to understand the initiation mechanisms in detail at the micro-interface level and support both models in terms of fundamentals of degradation and potential control actions.

IMPLEMENTATION STATEMENT

The project delivered the following categories: workforce development, technology development, education, and outreach activities. Currently, the project has provided funding to undergraduate and graduate students and postdoctoral researchers at Texas A&M University (TAMU), University of New Mexico, and Louisiana State University. Four undergraduate students (two females and two males) from TAMU Campus Galveston (TAMUG) have been recruited and trained to perform corrosion measurements and building of RC samples, as well as to produce the concrete specimens that were tested in this study. Also, conference papers summarizing the project's findings have been submitted this year: to the Construction Research Congress (CRC), the World Transport Convention, Tran-SET Conference, and the National Corrosion Association Engineers (NACE) Conference. Two peer-reviewed papers were submitted, and another peer-reviewed paper is under development for submission.

This project also offered summer internships: one included an undergraduate student from TAMUG, who actively participated in the continuous monitoring of RC structures. During this project, the current corrosion prevention and method classes at TAMU – Undergraduate (MSEN 446) and Graduate (MSEN 646) Course for Corrosion and Prevention Control – included the corrosion in RC structures topic. The class includes topics prepared in this project to be used to recruit students to transportation and the use of inspection tools for RC structures. Also, two seminars organized by the TAMU NACE Chapter, explaining the preservation of different assets and structures subject to environmental degradation, were offered to the community (including operators and companies) interested in corrosion and reliability of RC structures in Region 6. Students working on this project benefited from exposure to advanced modeling, mechanistic analysis, and linking laboratory samples within corrosive (atmospheric) environments, as well as real-time monitoring technologies that are not typical for traditional civil or materials engineers but will likely be part of the everyday life of future engineers.

From this point forward, the research team will promote the study's findings by developing educational materials on the production and use of corrosion rate measurements, which will be incorporated in materials science courses at TAMU and shared with other universities in Region 6, such as cases of study in journals or designed as a complement material for the mentioned courses The educational materials will also be summarized in the form of videos and presentations for dissemination to the department of transportation (DOT), courses related to corrosion and infrastructure and the transportation industry. The results of this work will be also be disseminated at peer-reviewed journals and national conferences, such as the NACE, the Transportation Research Board, and the American Society of Materials.

1. INTRODUCTION

Reinforced concrete (RC) structures are frequently exposed to aggressive environments that can deteriorate their structural properties and shorten their service life *(1)*. This exposure to aggressive environments can lead to corrosion of the reinforcing bars (rebars). The initiation of reinforcing rebar corrosion is controlled by the carbon/oxygen diffusion and aggressive species, such as sulfate and chloride, which penetrate through the concrete. If sulfate ions diffuse into concrete, they destroy the rebar by an ion exchange reaction *(2)*. While carbonation decreases the pH in the concrete, chloride ions promote the breakdown of the passive film, which is formed due to the highly alkaline pH of concrete on the reinforcing rebar and initiates localized corrosion at the rebar surface. Chloride ions can be introduced to the concrete in several ways: (a) admixture, (b) contaminated aggregates, (c) mix water, (d) salt water, and (e) atmosphere from coastal zones. Therefore, it is clear that chloride ions in the concrete and chloride-induced corrosion are unavoidable. This chloride-induced corrosion process, which is considered as one of the primary causes of degradation of RC structures, can cause reduction of the cross-sectional area of the reinforcing rebar and formation of voluminous corrosion products that typically induce cracking of the concrete structure and eventually spalling of the concrete cover, further exposing the embedded rebars *(3)*.

Construction methods, mathematical/analysis models, and design codes for the design of RC structures seem to be well-developed in the modern era of engineering. Safety, economic, and functionality requirements are heavily considered throughout the design process. Another important factor to consider when designing a structure is its durability. The durability of RC structures is strongly connected to degradation processes whose origin is environmental or functional. Among these processes is the development of corrosion on the steel reinforcement. Corrosion is a complex chemical or electrochemical process that leads to mechanical degradation of metallic materials *(4)*. Reinforcement corrosion has a direct effect on the durability of RC structures. Corrosion of reinforcing rebars is one of the major causes of deterioration of RC structures, affecting the useful service life of a given structure. Two types of corrosion, general and pitting, are possible. General corrosion affects the cross-section of reinforcement with nearly uniform metal loss over the perimeter of reinforcing bars. It also causes cracking and eventual spalling of the concrete cover and produces rust staining on the concrete surface, making it easily detectable during an inspection of the structure. Pitting, also referred to as localized corrosion, concentrates over small areas of reinforcement. Pitting corrosion often does not disrupt the concrete cover and produces little rust staining on the concrete surface, making it slightly more difficult to be discovered during inspections *(5)*.

In general, the mechanical degradation process of RC structures resulting from reinforcement corrosion can be divided into two stages: initiation and propagation. During the initiation period, chlorides infiltrate into the concrete cover by the diffusion mechanism. Over time, the chloride concentration grows until a threshold value is reached. Concrete provides physical and chemical protection to the reinforcing steel against penetrating chlorides, and as this threshold value is reached, it could lead to reinforcement depassivation *(6)*. Steel depassivation, implying the activation of the surface of steel rebar in RC, increases the risk of steel corrosion. The propagation period includes the development of corrosion (i.e., the period

in which the reduction of steel is detected). The propagation period is relatively short compared to the initiation period.

When corrosion occurs on the rebar, it is necessary to monitor the progress of corrosion kinetics, such that the failure of structures can be predicted or prevented. Corrosion monitoring is defined as collecting corrosion-related data on a regular basis that can be done on new or existing structures. Since corrosion cannot be completely stopped, corrosion always occurs even on fresh material or structures. This is the basic idea of conducting corrosion monitoring on new or fresh structures or rebar. In general, the electrochemical techniques for monitoring corrosion on the rebar can be divided into two main groups: (i) direct current (DC), and (ii) alternating current (AC) techniques. Each technique has its advantages and disadvantages. For the DC techniques, the measurement and apparatus are usually simple, but the information is limited. An example of this technique is a guard ring probe that is used to measure the corrosion current density (i_{corr}) of the rebar. In this technique, we measure the linear polarization of the rebar. By taking advantage of the Tafel constants, the i_{corr} or corrosion rate can be obtained. The electrochemical impedance spectroscopy (EIS) is based on AC. In principle, this method consists of superimposing a small (10–20 mV) AC signal on the electrochemical system of interest and measuring the response of the system to this perturbation. This technique is sophisticated and usually requires a good knowledge of mathematics. An advantage of this technique is that, if the data is treated properly, it can offer comprehensive information about the kinetics on the rebar/concrete interface.

To simulate the chloride entrance and its transport into concrete pores, Fick's diffusion laws have generally been considered adequate models. It should be noted that Fick's laws pertain to homogenous, isotropic, and inert materials, while concrete is distinguished as a heterogeneous, anisotropic, and chemically reactive material. Though contradictory, the methods commonly adopted for chloride transportation modeling in concrete consider this process to be governed by ionic diffusion only. Also, taking into account that the concrete cover is assumed to be mostly saturated, the hypotheses of Fick's laws are considered acceptable for the chloride ingress modeling, especially in the corrosion initiation stage *(7)*.

To determine the time to corrosion initiation, the one dimensional Fick's second law, which describes chloride diffusion, is commonly used *(8)*. In the diffusion of chloride into concrete, the chloride concentration C at depth x with time t takes the following form:

$$C(x,t) = C_s[1 - \text{erf}(\frac{x}{2\sqrt{Dt}})] \qquad [1]$$

where:
C_s = the surface chloride concentration with units of % mass,
erf = the statistical error function, and
D = the diffusion coefficient with units of mm^2/yr.

The time variable t is defined as the period of time from the samples exposed to the marine environment to the specific future time of interest. It is assumed that the corrosion initiates at time T_{corr} when the chloride concentration at depth d_c reaches to the critical chloride concentration, C_{cr}.

In the solution of this one dimensional Fick's second law by $C(d_c, T_{corr}) = C_{cr}$, the diffusion coefficient *D* is known to be dependent to the concrete material conditions, such as the water-to-cement ratio, and exposure conditions, such as the surface chloride concentration *(9, 10)*. Duracrete *(11)* suggested the probabilistic model form for the chloride induced corrosion initiation time, which considers the concrete materials and exposure conditions. In this research, we similarly develop the probabilistic model. Instead of maintaining all of the parameters, we focus on developing the most effective model by selecting the most accurate model with the least number of parameters using model selection criteria described in the later section. We transform the function using the log-transformation of the model defining *D* as:

$$\log[D(t,\Theta)] = \log[D'(t,\theta_C,\alpha_C)] + \sigma\varepsilon \qquad [2]$$

where:
$\Theta = (\theta_C, \alpha_C, \sigma)$ denote the sets of unknown parameters to be estimated using Bayesian methodology,
$\theta_C = (\theta_1, \theta_2 \ldots)$ represents the unknown parameter representing the diffusion coefficient for the reference case, and
$\alpha_C = (\alpha_1, \alpha_2, \ldots)$ is the set of parameter correction factors considering various material and exposure conditions, which also can be estimated using Bayesian methods.

In this research, α_1 has been used for the correction factor for various water-to-cement ratios and α_2 for the correction factor for the concrete curing days. One can develop models by expanding the model with additional correction factors $\alpha_3, \alpha_4, \ldots$ for further available parameter conditions. σ is the model standard deviation and ε is the random variables, which mean equals zero and the standard deviation is 1. The logarithm transformation results in the model uncertainties $S = exp(\sigma\varepsilon)$ with the expression of the original diffusion equation as $D(t,\Theta) = D'(t,\theta_C,\alpha_C) \cdot S$.

In this study, the candidate models for the diffusion coefficient to solve the time to corrosion initiation time, T_{corr}, has been selected as the following:

Model A: $D'(t,\theta_C) = \theta_1(\theta_2/t)^{\theta_3}$ [3]

Model B: $D'(t,\theta_C,\alpha_C) = \alpha_1\theta_1(\theta_2/t)^{\theta_3}$ [4]

Model C: $D'(t,\theta_C,\alpha_C) = \alpha_1\alpha_2\theta_1(\theta_2/t)^{\theta_3}$ [5]

Model A assumed that the effects of the material conditions on the diffusion process are negligible, which will be used as a reference case only for this research. Model B assumed the concrete curing time has no significant effect on the diffusion, and Model C assumed that both the water-to-cement ratio and the concrete curing time significantly affect the diffusion process. The models result in a solution to the Fick's law, as follows:

Model A: $T_{corr,A} = [\frac{d_c^2}{4S\theta_1(\theta_2)^{\theta_3}}[erf^{-1}(1-\frac{C_{cr}}{C_s})]^{-2}]^{1/1-\theta_3}$ [6]

Model B: $T_{corr,B} = [\frac{d_c^2}{4S\alpha_1\theta_1(\theta_2)^{\theta_3}}[erf^{-1}(1-\frac{C_{cr}}{C_s})]^{-2}]^{1/1-\theta_3}$ [7]

Model C: $T_{corr,C} = X[\frac{d_c^2}{4S\alpha_1\alpha_2\theta_1(\theta_2)^{\theta_3}}[erf^{-1}(1-\frac{C_{cr}}{C_s})]^{-2}]^{1/1-\theta_3}$ [8]

In this research, the unknown parameters are estimated based on sets of experimental data using Bayesian updating methods. In the corrosion initiation estimation, the time-dependent variation of the surface chloride concentration estimation has not been considered.

In this study, we use a similar approach to assess the reliability of corroding RC beams with the goal of being able to predict the remaining service life. The design life of an RC structure subjected to corrosion was examined in this study using a probabilistic framework for the flexural behavior of a beam by evaluating the reliability concrete structures subjected to uniform corrosion using the First Order Reliability Model (FORM). The proposed framework is envisioned to help infrastructure owners in making maintenance and repair decisions by comparing alternatives based on target reliability thresholds and target service life.

2. OBJECTIVE

The objective of this study is to design and generate a comprehensive framework for corrosion assessment in RC that will provide an effective approach to monitor and quantify damage evolution due to corrosion, as well as will provide efficient and cost-effective maintenance/repair strategies by incorporating the corrosion monitoring observation to the structural design process. Specific objectives:

- Use reliable monitoring and characterization technologies that helps to validate the theoretical models used for corrosion assessment and reliability.
- Design an electrochemical set up for qualitative/qualitative characterization of corrosion in reinforced concrete interface.
- Develop mathematical model based on deterministic/probabilistic approach.
- Develop a basis for predicting the integrity of the RC structures in aggressive structures by using monitoring tools, data analysis, mathematical modeling, cost effective control/repairing actions

3. SCOPE

This research project will develop a framework system for corrosion-damaged RC elements so that the current bridge inspection and management protocol can be improved to have a more robust tool. Also, an important class of physical assets – RC bridges – can be preserved and be more reliable by controlling, managing corrosion in a cost-effective way. One of the center's stated objectives is to extend the life of the existing or new transportation infrastructure through the reliability of the elements of a reinforced structure. This work provided the combination of monitoring tools based on two different principles; the first principle covers the corrosion rate measurement and the second the mechanistic processes for degradation mode. The framework included the following activities: theoretical tools and experimental results, the results for this research provided methods for scientific assessment of remaining service life and robust degradation principles design for repair of critical RC structures exposed to corrosion environments. This research aims to address two important missions for Tran-SET Regional Center and DOT: (a) preserve what we have – by providing best practice tools for preserving physical infrastructures and extending their service life and (b) implement a decision support system that helps streamline infrastructure operations.

4. METHODOLOGY

To meet the main aim of this study, which is to provide a comprehensive framework for predicting the reliability of concrete structures, a set of experimental and modeling work was performed. The experimental part consists of: (a) i_{corr} (corrosion current) measurement that was performed at a Mexican location near the Gulf of Mexico prior this work and (b) EIS testing (characterization) that was done at the USA location near the Gulf of Mexico. These two sets of results support the development for the reliability model and the mechanistic degradation process of the RC samples. There were different tasks during this work, the data collection, design of experimental set up, theoretical development based on the collected information, and results are presented as follows:

4.1. Collecting Atmospheric Conditions and Analyzing Damage Evolution

4.1.1. Utilizing Existing Results Performed at Yucatan Peninsula

Before this work, the following parameters were considered for the concrete samples design for the long-term testing. A total of 180 datasets were used for the corrosion initiation model development, which was collected from the tropical marine environment of the Yucatan Peninsula, Mexico, over 10 years and previously reported in several publications *(12 – 14)*. The samples were prepared by crushed limestone aggregates with Portland cement. Each concrete sample had a cylindrical shape with a diameter of 75 mm and 150 mm in height. Figure 1 shows a schematic description of the samples configuration and design used in the data collection procedure. Data was collected for samples with five *w/c* ratios (0.46, 0.50, 0.53, 0.70, and 0.76) and three lengths of curing (i.e., 1, 3, and 7 days). To prevent chloride entrance from the top and bottom flat of the samples, the parts were sealed with epoxy coatings. More experimental details, including the procedure of collecting chloride concentration data for different depth and time, are illustrated in previous studies by Castro et al. *(13 – 15)*. The range of data used for this research is provided in Table 1.

Table 1. Range of properties of the concrete sample.

Variable	Symbol	Range
Concrete Strength	f_c'	14.7 – 34.3 MPa
Curing days	Cd	1 – 7 days
Water-to-cement ratio	w/c	0.46 – 0.76
Distance from shore		Coastal (50 – 100 m)

The team collected the data extracted from experimental testing from the Gulf of Mexico location; the information was generated and taken for more than 60 months prior to the initiation of this project. The mechanistic analysis included the inherent parameters of the concrete, considering the initial conditions and the parameters that evolve with time. All information was summarized for all measurements and parameters that can be quantified and estimated with commentaries for suitability and applicability for various project conditions and objectives.

4.1.2. Preparing and Testing Samples for Further Analysis (Mexico, Merida and Galveston, TX)

Different geometry and configuration were design and during this project to characterize the transport and interfacial processes occurring during the degradation mechanism. One set will be set in Mexico, Merida, the second set was located in Galveston, Texas. The design includes the following:

The cement used was Portland Type I Holcim Apasco (CPC 30R); this is common for industrial applications because of its mechanical resistance, sulfates, and the low reactivity with the alkali-aggregate. The aggregates used are canter coarse particles of calize rock with a maximum size of 20 mm and most suitable granulometry, with a loss of abrasion of 35% and fine aggregate with a small excess of fine particles (very typical for this materials). The water used was from the location (no special requirements). To study the influence of depth on the corrosion of reinforcing steel bars, the rebar was embedded at three different locations from the concrete surface (as illustrated in Figure 2), with cover depths of 1.5, 2.0, and 3.0 cm. To prevent chloride entrance from the flat top and bottom surfaces of the sample, those two parts were sealed with epoxy coatings.

Concrete prisms with a dimension of 30 × 15 × 15 cm were made for corrosion testing. In each sample, there are six rebars: two 1.5 cm deep, two 2.0 cm deep, and two 3.0 cm deep. The working area of each rebar exposed to concrete is 47 cm^2 (Figure 1). The *w/c* ratios are 0.45 and 0.65. Three samples have a ratio of 0.65 *w/c*, and the other three have a ratio of 0.45 *w/c*. Only two w/c ratios are included in this work. The lowest magnitude w/c ratio is equivalent to the previous samples exposed for several months prior to this project. This latter ratio illustrates low water content and more realistic magnitude for RC structures. One side of each sample is exposed to predominant winds and the other side to non-predominant winds.

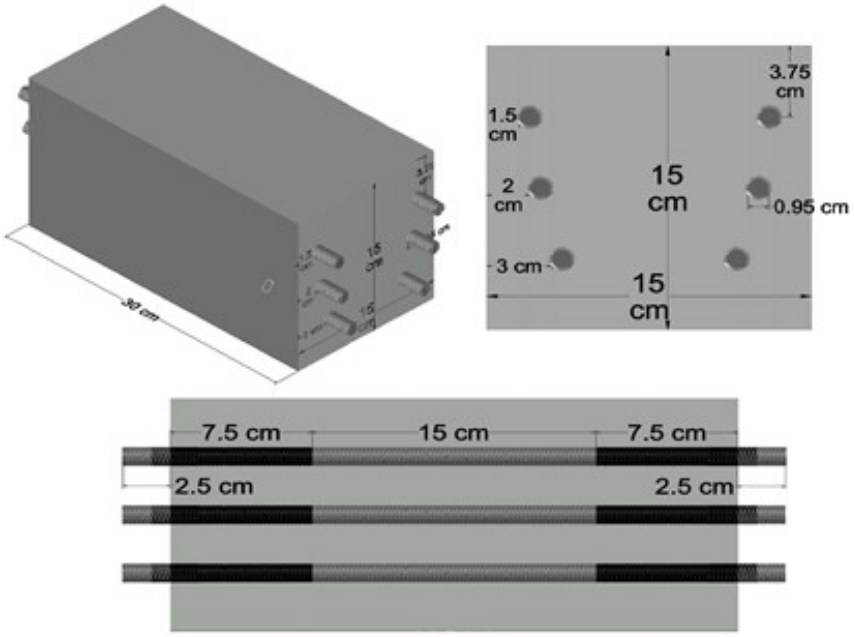

Figure 1. A concrete sample configuration with six rebars.

Mexico Samples: Figure 2 shows 18 total samples in Mexico, Merida. Eighteen samples were subjected to corrosion rate (i_{corr}) measurement using a guard ring sensor (Figure 3). The rationale to have the samples include the following parameters and configurations: Six samples were used for electrochemical measurements for characterization of the rebar dissolution mechanisms, 6 samples included the chloride profile for the deterministic and probabilistic estimation based on damage approach and the last six batch was used to expose in urban environment and characterize the electrochemical response of the samples in drier environment. For the electrochemical measurements, a lead from the device is connected to the rebar that's corrosion rate needs to be measured, while the other lead goes to the probe. The measurement of the actual chloride concentration at a different depth was performed by cutting the top part of the duplicate sample without the rebar. Then, the concrete powders of different depths were collected by drilling, and the chloride concentrations were determined by the ion-selective electrode.

Figure 2. Concrete samples in the seacoast exposure in Mexico.

Figure 3. In situ i_{corr} measurement using a ring probe.

Galveston, TX Samples: Six RC samples were sent to Galveston for corrosion testing and electrochemical characterization. The samples sat on a table during corrosion testing (Figure 4). To avoid parallel impedances, the samples were lifted off of the table surface, and pegs

were inserted between the concrete and table surface (Figure 4). The position of the samples was set for predominant winds and non-predominant winds at 1m from the shore based on the direction of the wind. The direction of the wind was predetermined with windmill anemometer and previous wind charts from Galveston area. The neoprene tubing is applied to one side for protection; the other side was used to take the measurements. A conductive elastomer was laid on the surface of the concrete, covering the top and sides, and an aluminum metal sheet (acting as a counter electrode on a two-electrode system designed to fit on the elastomer) was placed on it. The metal sheet was tightened down by metal rings to compress it onto the concrete, as shown in Figure 5.

Figure 4. Concrete prism samples in the seacoast exposure in Galveston.

Figure 5. Concrete prism sample covered by the aluminum electrode.

The information relevant to the kinetics on steel reinforcement/concrete interface was explored in more detail by performing the EIS testing. In this testing, this aluminum sheet (along with

the conductive elastomer) acts as a counter electrode. The EIS testing was performed at 0 V (not bias potential) versus OCP from 1000 kHz to 0.01 Hz with an amplitude of 10 mV.

4.2. Algorithm for the Unification Model (Deterministic-Probabilistic) from Collected Parameters

By following the proposed framework, a probabilistic model of diffusion-based corrosion initiation was developed using experimental data exposed to the coastal atmospheric environments. The methodology for collecting and gathering the information is the first step among three for the deterministic-probabilistic approach of the damage evolution, as illustrated in Figure 6.

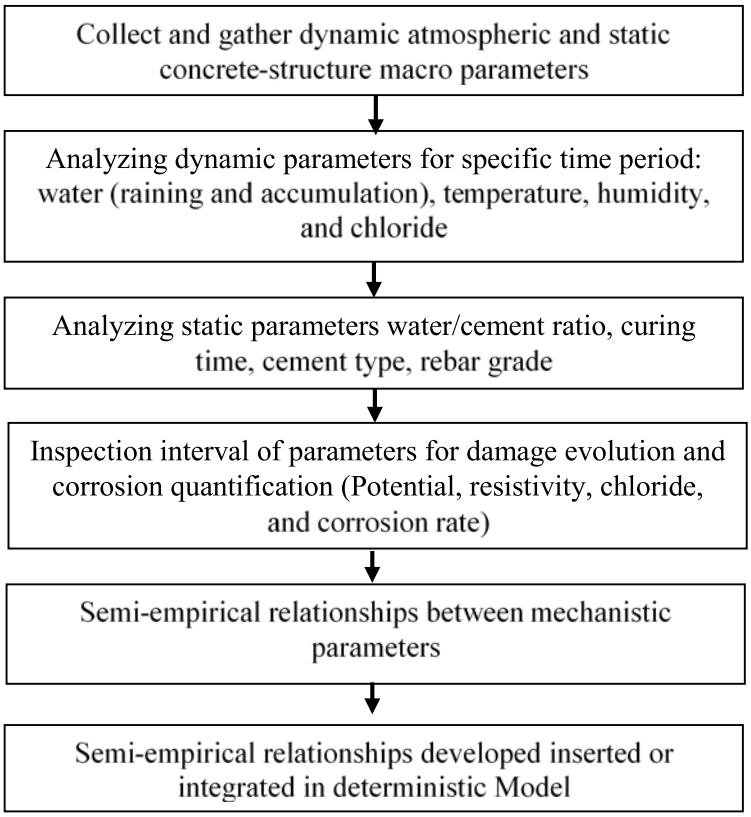

Figure 6. Steps for the unification of deterministic-probabilistic approach from the collected data.

4.3. Developing Deterministic and Probabilistic Models

4.3.1. Deterministic Modeling Approach

The theoretical deterministic modeling with RC elements and electrolyte is developed based on trasnmission line concept. The measurements based on rebar/concrete interface real-time monitoring in corrosive environments helped to validate the deterministic approach, the division of the elements in the RC system is illustrated in Figure 1.

The deterministic model includes: the subdivision of the entire system into equal geometries to characterize and quantify the charge carrier (corrosion precursors), making the concrete/rebar divisible into similar-elements; thus, the breakthrough of deterministic concept

by theoretical and testing magnitudes platform could be achieved. TLM included the interfacial phenomena and mechanisms with the spatial speciation distribution within the concrete. TLM helped to characterize the mass and charge transfer mechanisms, and interfacial degradation processes with time. TLM describes ionic and electron transport in homogeneous/heterogeneous structures (Figure 7).

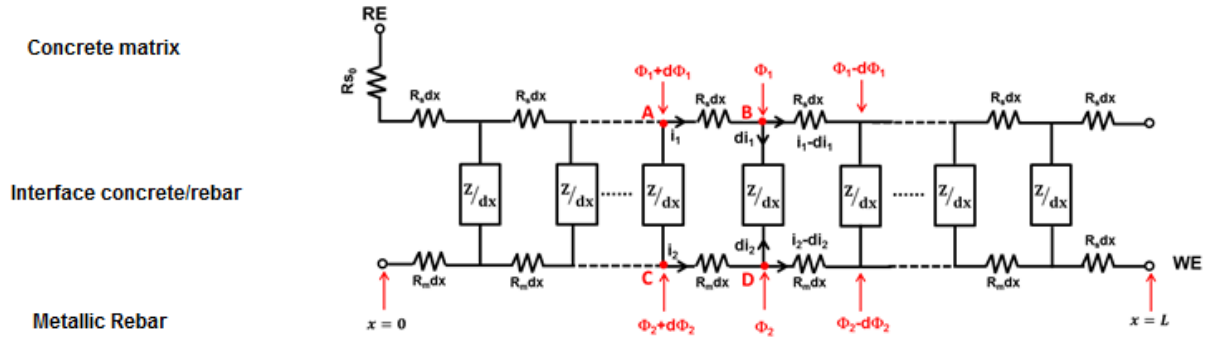

Figure 7. Transmission line model of reinforced concrete under a corrosive environment

4.3.2. Probabilistic Modeling Approach

We performed comprehensive reliability-based modeling for corrosion initiation, corrosion damage monitoring, and repair design of RC structures. It was assumed that corrosion of reinforcement would be initiated when the chloride concentration at the interface between the concrete matrix and rebar exceeds the critical chloride value. Estimating the chloride concentration depends on different depth and time, such a model was designed based on the Fick's second law. The model also includes the effect of various water-cement ratios and curing days. These conditions were designed to affect diffusivity through multiple parameters, such as α_1 and α_2. The model selection criteria of AIC (Akaike information criterion) and BIC (Bayesian information criterion) were also applied to help with the model selection process by comparing the qualitative effect of each α_1 and α_2 on the model. Sensitivity and importance of variability analyses were also performed to identify the parameter that is the most important source of uncertainty and, thus, can influence on the model reliability.

For the corrosion damage monitoring model, which can include not only corrosion initiation but also the corrosion propagation, the corrosion current value, i_{corr}, was designed to consider both water-cement ratios and time since the corrosion initiation. The corrosion current was also correlated with the diameter and area of the reinforcement. As such, the dimension change of the reinforcement directly affects the concrete mechanical property. Therefore, the model was also designed to reflect the change of both flexural strength and load resistance based on the limit state functions.

Throughout the probability modeling process, the FORM was applied to estimate the probability of corrosion initiation and the probability of mechanical failure with their reliability index, β. The service life predictions depend on the repair designs (which include restoring β value), degradation rate, and different initial β value.

The first modeling we performed was based on the surface chloride concentration data from previous experimental work. This research utilizes the probabilistic methods to identify and predict the uncertainties involved in the system and to provide reliability prediction. The Bayesian methodology was used in the evidence-based models using the experimental data. The impacts of each parameter, including material properties, environmental conditions, and the structural geometries, were investigated, also considering the uncertainty within the system.

To determine the concentration profile in different depth and time, the model is based on the diffusion equation, which is fundamentally based on the Fick's law (Equation 1). A statistical approach was added using a Bayesian updating technique to decide the model parameters. The model parameters, θ_1, θ_2, and θ_3, were estimated by the maximization function that maximizes the concentration profile likelihood when a previous reference case data set was given. The reference case was chosen as *w/c* = 0.46 with *Cd* = 7. Section 1 describes the three candidate models for the diffusion coefficient to solve the time to corrosion time, T_{corr}; however, they are replicated and discussed in greater detail below beginning with Model A.

$$\text{Model A: } D'(t, \theta_C) = \theta_1(\theta_2/t)^{\theta_3} \quad [3]$$

where:
t = Time (month), and
$\theta_1, \theta_2, \theta_3$ = parameters in the diffusion model.

Table 2 shows the posterior statistics of the parameters for the chloride diffusion Model A using the reference case of *w/c* = 0.46 and 7 days of curing, based on the diffusion equation without the correction factor. The sigma (σ) value represents the model error. The correlation coefficient shows how the parameters are correlated with each other, and possibly indicate the importance of each parameter. In this case, θ_2 and θ_3 show relatively higher correlation compared to the other parameters' correlations, indicating that those two parameters are possibly merged to increase the equation efficiency; nevertheless, there is also another possibility – that such a merging process increases the model uncertainty. It was observed that the model has low statistical uncertainty from the generally low standard deviation values.

Table 2. Posterior statistics of the parameters in a diffusion model.

			Correlation Coefficient			
Θ	***Mean***	***St. dev.***	$\boldsymbol{\theta_1}$	$\boldsymbol{\theta_2}$	$\boldsymbol{\theta_3}$	$\boldsymbol{\sigma}$
$\boldsymbol{\theta_1}$	46	1.001	1	-	-	-
$\boldsymbol{\theta_2}$	1.88	0.339	-0.046	1	-	-
$\boldsymbol{\theta_2}$	5.47	1.006	0.008	-0.597	1	-
$\boldsymbol{\sigma}$	0.008	0.002	-0.031	-0.014	-0.153	1

To express the different concrete conditions compared to the reference case, the correction factors, α_1 and α_2, were added to the diffusivity equation (Tables 3 and 4). The correction factor helps improve the model fit to the given data set and reflects the trend that might not be observed in the posterior statistics with the reference case. Each α_1 and α_2 represents the *w/c* correction factor and *Cd* correction factor, respectively. The first element added to the reference case was α_1 (Model B).

Model B: $D'(t, \theta_C, \alpha_C) = \alpha_1 \theta_1 (\theta_2/t)^{\theta_3}$ [4]

Table 3. w/c correction factor, α_1.

Model	Distribution	α_1 Mean	α_1 St.dev
$w/c = 0.46$	Normal	1	0.400
$w/c = 0.50$	Normal	1.719	0.576
$w/c = 0.53$	Normal	2.283	0.673
$w/c = 0.70$	Normal	2.678	
$w/c = 0.76$	Normal	2.783	0.984

Similar to the correction factor for the different *w/c* ratio, α_1, the correction factor for the different *Cd*, α_2, was also inserted to the diffusivity equation to reflect the effect of different concrete curing days to create Model C. Such a correction factor was inserted after the α_1 was added, so that both correction factors coexist. However, unlike α_1, α_2 did not show a direct relationship between the concrete curing days and the diffusivity (Table 5). This trend might be interpreted in multiple ways: as the α_1 affecting the α_2 trend; that the impact that comes from the different *w/c* ratios dominates the impact from the different *Cd*; or because of the impact of outlier data within the given data sets.

Model C: $D'(t, \theta_C, \alpha_C) = \alpha_1 \alpha_2 \theta_1 (\theta_2/t)^{\theta_3}$ [5]

Table 4. Curing days correction factor, α_2.

Model	Distribution	α_2 Mean	α_2 St.dev
$Cd = 1$	Normal	1.265	0.221
$Cd = 3$	Normal	0.716	0.073
$Cd = 7$	Normal	0.875	0.090

To determine how those two correction factors affect to the equation efficiency, the two model selection criteria, Akaike Information Criterion (AIC) (Equation 10) and Bayesian Information Criterion (BIC) (Equation 11) were applied. Those two criteria measure the trade-off between model complexity and the fitting quality based on the number of unknown parameters and the size of the data samples. A comparison of the two model equations for each criterion helps the comparison of the efficiency and the likelihood of each model equation. From Table 5, there is no substantial equation efficiency between the two model equations. However, the equation without the curing day correction factor, α_2, shows a much higher likelihood as it gives much lower AIC and BIC values. This means that the results from the equation without the α_2 represents the values with higher reliability. Therefore, from hereon, the results only show the case of the diffusivity without the α_2.

$\text{AIC} = -2\log[L(\Theta_k|G_k)] + 2N_P$ [9]

$$\mathrm{BIC} = -2\log[L(\Theta_k|G_k)] + N_P \log N_S \quad [10]$$

where:

$L(\Theta_k|G_k)$ = likelihood function,
Θ_k = unknown parameter values,
G_k = data points,
N_P = number of unknown parameters, and
N_S = sample size.

Table 5. Model selection criteria for candidate models.

Model	N_p	AIC	BIC
$D = \alpha_1\theta_1(\alpha_2\theta_3)^{\theta_2}$	*5*	*–410*	*–401*
$D = \alpha_1\theta_1(\theta_3)^{\theta_2}$	*4*	*–1306*	*–1294*

4.4. Developing Reliability-Based Service Life Prediction Model

4.4.1. Integration of Deterministic with Probability

Typical concrete deterioration is gradual; and depending on their service and environment, steel RC structures can theoretically stand for decades before the onset of steel corrosion. To understand how corrosion affects the RC structures, it is beneficial to understand the deterioration process corrosion undergoes from a mechanistic point of view. For reinforcing steel to corrode, the passive oxide layer on the steel must fail. If the concrete cover that protects the reinforcing steel is damaged, and the bond between the concrete and steel reinforcing bars fails due to dissoution, the steel's passive layer will breakdown, and active corrosion of the steel will start. There are two mechanisms that will damage the steel's passive layer even if the concrete cover is not damaged: chloride ions (Cl^-) and carbonation *(16)*. In this work, we considered the chloride attack as the main treat for corrosion damage. The parameters should be identified by deterministic and mechanistic processes.

Chloride-induced corrosion is a major problem for aging concrete highway bridge structures, particularly in marine environments or areas where road salts are used *(16)*. Chlorides can be cast into concrete during the mixing process or diffuse in from the external environment. When the chlorine ions reach the reinforcing steel, they can penetrate the passive oxide layer and cause a defect. A build-up of these chlorine ions can cause the steel's passive oxide layer to break down, which allows corrosion to initiate *(16)*.

Chloride diffusion is documented as one of the major factors that trigger corrosion. Therefore, accurately modeling for the chloride diffusion was essential to better evaluate the corrosion of the RC samples. Subsequently, design criteria can be more realistically proposed to assure safety and economic standards into the design of RC structures. Due to the inherent randomness regarding chloride diffusion and corrosion, these processes should be properly modeled using deterministic-probabilistic approaches *(5)*.

4.4.2. Service Life Prediction Based on TLM (Deterministic)

Deterministic corrosion model: Based on the TLM, different conditions were characterized by different parameters, such as the outcome of the corrosion process or RC activation/degradation process. The following figures illustrate the different profiles based on the chloride content within the reinforced matrix.

We could identify critical parameters affecting the chloride content. Figure 9 shows the diffusion coefficient influence in the chloride profile within the concrete matrix. The magnitude of the coefficient is proportional to the amount of chloride accumulated within the concrete matrix. Coefficients in the order of $1x10^{-5}$ cm^2/sec is the highest magnitude before the concrete is supersaturated with electrolyte. Diffusion coefficient correlates with the porosity, quality of the concrete and processing parameters. The estimation does not consider specific property only the general characteristic of the concrete. The estimation was based on the current and impedance generated due to the conditions of the concrete.

Figure 10 shows the lifetime expectancy based on the corrosion of the rebar due to the chloride accumulation and presence within the rebar/concrete interface. TLM could demonstrate the lifetime prediction by assuming the dissolution of the rebar represents the failure mode of the element. The number of years was estimated based on the chloride accumulation and content within the concrete. The estimation includes the impedance and corrosion rate magnitudes for different chloride content within the concrete. The higher the chloride content within the concrete matrix, the life expectancy of the rebar decrease from 15 years (for high concentration) to 45 years at low chloride concentration. Deterministic modeling is limited due to the assumptions considered for the calculation, such as contact parameters with time.

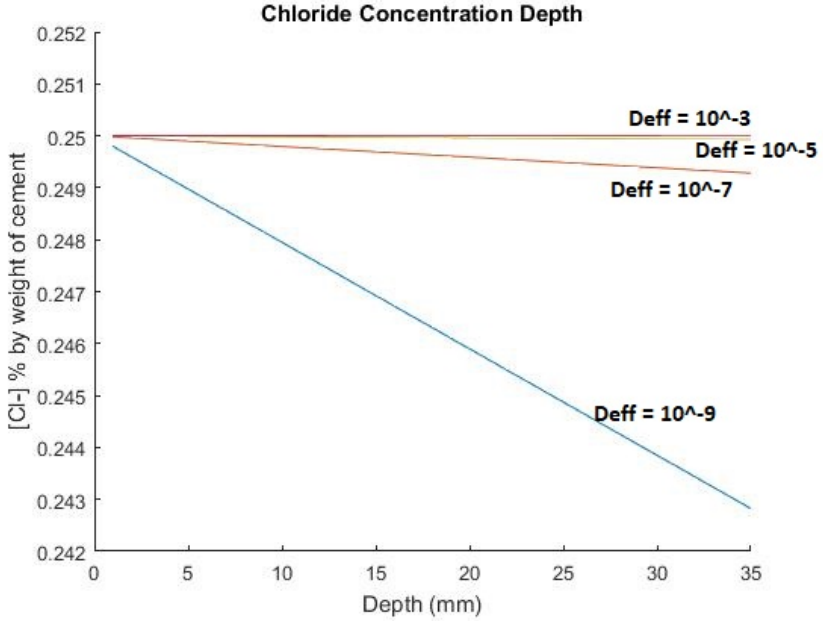

Figure 8. Changing effective chloride diffusion coefficient.

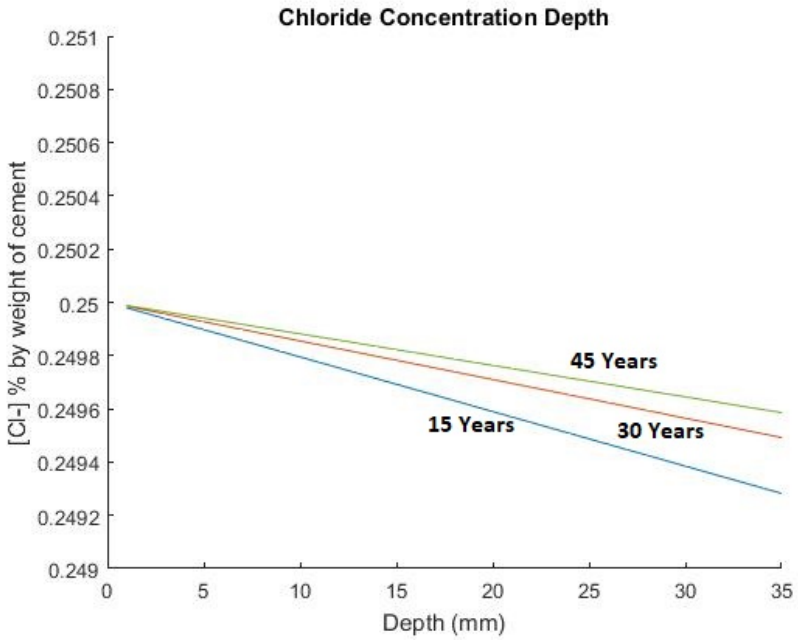

Figure 9. Changing the time of exposure of the reinforced structure.

4.4.3. Service Life Prediction Modeling (Probabilistic)

Probabilistic Corrosion Model: Structural reliability and risk analyses aim to quantify the probability of failure due to uncertainties. These uncertainties in a system vary from design to manufacturing to environmental conditions. The modeling of structural systems considering these uncertainties has become useful regarding the durability of a structure. Probability models can embrace knowledge from multiple fields to allow for a more consistent, comprehensive, and dependable understanding concerning the reliability of a structure, as opposed to using a purely deterministic approach. Through statistical associations, this method acknowledges the addition of uncertainties in numerous analyses in a consistent theoretical manner *(6)*. With an understanding of the corrosion process, as well as basic chemical and RC concepts, reliability algorithms can be established and analyzed using numerical simulation techniques, such as FORM procedures. These numerical simulation techniques can determine the probability of structural failure. The approximation of structural failure probability can be used for estimating the performance and lifetime of structures.

First Order Reliability Model: The FORM is an advanced mathematical method for assessing the probability of failure, P_f, of a structural component. In this method, P_f is often expressed in terms of the reliability index, β. The relationship between P_f and β is given by:

$$P_f = \Phi(-\beta) \qquad [11]$$

where:
$\Phi(X_i)$ = the cumulative distribution function or CDF for a standard form of a normal distribution ($N[0,1]$).

Assessment of the probability of failure is based on the transformation of the limit state function to a standardized system, where the random variables are transformed to a

standardized space of normally distributed variables *(17)*. Standard normal variables have a mean of zero and a standard deviation of 1. A non-normal random variable, X_i, is reduced to a corresponding random variable, Z_i, by:

$$Z_i = \frac{X_i - \mu_{X_i^e}}{\sigma_{X_i^e}} \quad [12]$$

where:
Z_i = a random variable characterized by a probability density function with mean equal to zero and a unit standard deviation,
$\mu_{X_i^e}$ = equivalent mean of a random variable, and
$\sigma_{X_i^e}$ = equivalent standard deviation of a random variable.

$$\mu_{X_i^e} = x^* - \sigma_{X_i^e}[\mathbf{\Phi}^{-1}(F_X(x^*))] \quad [13]$$

$$\sigma_{X_i^e} = \frac{1}{f_X(x^*)}\varphi[\mathbf{\Phi}^{-1}(F_X(x^*))] \quad [14]$$

The equivalent mean and standard deviation, $\mu_{X_i^e}$ and $\sigma_{X_i^e}$, for each non-normal random variable has to be evaluated multiple times and the design point, x^*, is determined iteratively until convergence. These are determined using Equations 13 and 14 where $F_X(x^*)$ is the cumulative distribution function of the non-normal random variable evaluated at the design point, and $f_X(x^*)$ is its probability density function evaluated at the same design point, x^*.

The reliability index is defined in the new standardized, reduced space; as the minimum possible distance between the origin and the limit state function. The minimum distance point on the limit state surface is defined as the design point, x^*, and represents the most probable point of failure in the design space. For simplicity, the initial design point is often assumed to be the mean values of each random variable. The direction of cosines was used to estimate the sensitivity of each variable and to identify a new design point for each parameter in each respective iteration. The reliability index, β, is determined using this iterative method in an incremental way rather than solving the whole problem in each iteration. The iterative process ends once β has converged, which is defined as obtaining incremental values for β that are smaller than a user specified tolerance, taken as 10^{-4} in this study. More details about FORM can be found in the work of Nowak and Collins *(18)*. Even though convergence to the global minimum is not guaranteed using this method, it is the experience of the second author that this is not an issue for various structural concrete applications *(19-21)*.

Limit State Function: The nominal flexural strength of a concrete beam with a rectangular cross section is given by:

$$M_n = A_s\, f_y\left(d - \frac{A_s\, f_y}{1.7 b f_c'}\right) \quad [15]$$

where:
f_c' = the concrete compressive strength,
f_y = the steel yield strength, and

d = the effective depth of the steel reinforcement.

The required nominal resistance is determined using Load and Resistance Factor Design (LRFD) equations *(19)* to meet the nominal demands imposed by dead and live loads ($M_{n,D}$ and $M_{n,L}$), which are assumed to be a 1:1 ratio for simplicity.

$$\phi M_n \geq \gamma_D * M_{n,D} + \gamma_L * M_{n,L} \quad [16]$$

In the design equation, the load factors γ_D and γ_L can be taken as 1.25 and 1.75, respectively, for transportation structures according to AASHTO-LRFD *(22)*, and the resistance factor, ϕ, is taken as 0.9 for RC structures.

The limit state function for flexural capacity can be written as:

$$g(\,) = M_r - (M_D + M_L) \quad [17]$$

where:
M_r = the flexural resistance of the beam and
$(M_D + M_L)$ = the flexural demand from the applied external dead and live loads.

The uncertainties of characteristic and experimental parameters regarding Equation 17, the following probabilistic model was developed by Ghanooni-Bagha *(23)* and employed for this study as well.

$$g(\,) = \xi_M(A_s(t)f_y(t)(d - K\frac{A_s * f_y(t)}{b * f_c^{'}})) - (M_D + M_L) \quad [18]$$

$$f_y(t) = (1 - \gamma\frac{A_s - A_s(t)}{A_s}) * f_y \quad [19]$$

In the limit state function given by Equation 19, $f_y(t)$ is considered as the yield stress of corroded steel bars. This stress is linearly correlated with the un-corroded steel bars yield strength. The γ coefficient is an experimental parameter with a mean of 0.5 and a Coefficient of Variation (COV) of 12%. The professional factor, ξ_M, is a random variable representing the accuracy of the flexural resistance model.

5. FINDINGS

The results of this study are divided into two main categories: (i) experimental and (ii) modeling. The results from the experimental part include the previous data set from previous project of corrosion rate (represented by i_{corr}) obtained from the Mexico location and the second set included generated EIS data from the Galveston, USA location. From this set of data, the modeling was developed and verified to predict the reliability of the concrete structures. The first set of data were used to develop the probabilistic approach and the second set was to be used as support for the degradation mechanisms for each model. The findings are described as follows:

5.1. Analysis of Results for Reliability-Based Model

5.1.1. Damage Evolution for Samples Exposed in Mexico

Figures 10–12 present the i_{corr} value evolution for the long-term exposure samples with different casted *w/c* ratios measured for 1, 3, and 7 days of curing, respectively. In general, the effect of days of curing on corrosion behaviors of rebars is not significant, as evident by the similar i_{corr} trends for all samples with different days of curing. The i_{corr} values tend to increase with time and are located in the high corrosion rate region after 60 months of exposure. In contrast, the influence of the *w/c* ratio on corrosion rate is more pronounced.

For samples cured for 1 day (Figure 11), all samples show an increase in i_{corr} with increasing time, indicating an increase in corrosion rate. We detected differences in samples with a high *w/c* ratio, which tend to have higher i_{corr} during the first 50 months of exposure. Following the 50 months, there is a higher variability for the same magnitude. During this 50 month period, the highest i_{corr} was found in the sample with the highest *w/c* ratio (0.76), while the lowest i_{corr} was detected in the sample with the lowest *w/c* ratio (0.46). However, the i_{corr} values of high *w/c* ratio become lower after 50 months. In contrast, in this period (after 50 months), the samples with the low *w/c* ratio becomes more active, as indicated by its higher i_{corr}. For the initial 10 months, all samples are in the passive condition (i_{corr} < 0.1 μA/cm^2), and then corrosion activity becomes more active as indicated by an increase in i_{corr}, except for the sample with the lowest *w/c* ratio, which shows passivity extension until 20 months. After 20 months, the corrosion rate for all samples is high (i_{corr} > 1 μA/cm^2). Similarly, all these behaviors are also observed for samples cured for 7 days (Figure 12).

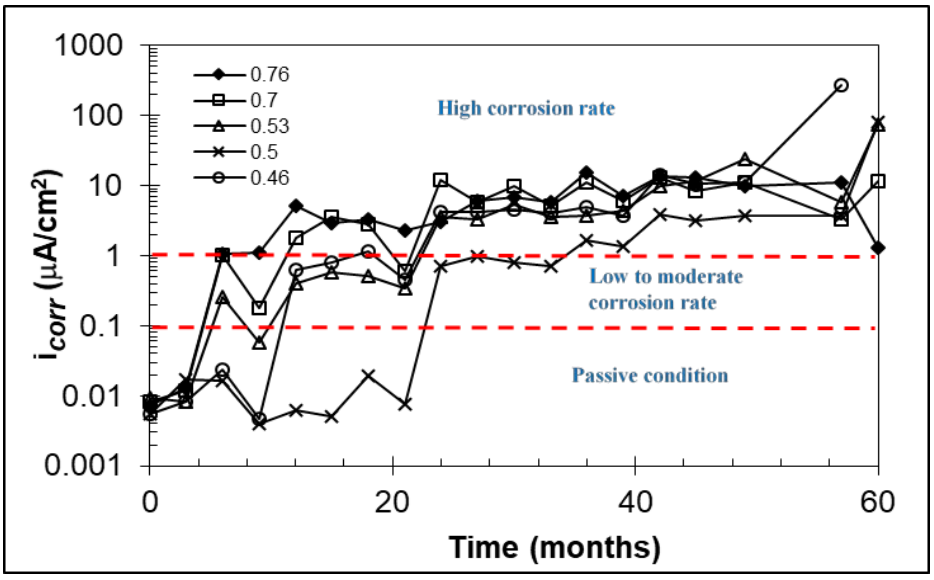

Figure 10. i_{corr} evolution of samples with various *w/c* ratio after 1 day of curing measured for 60 months.

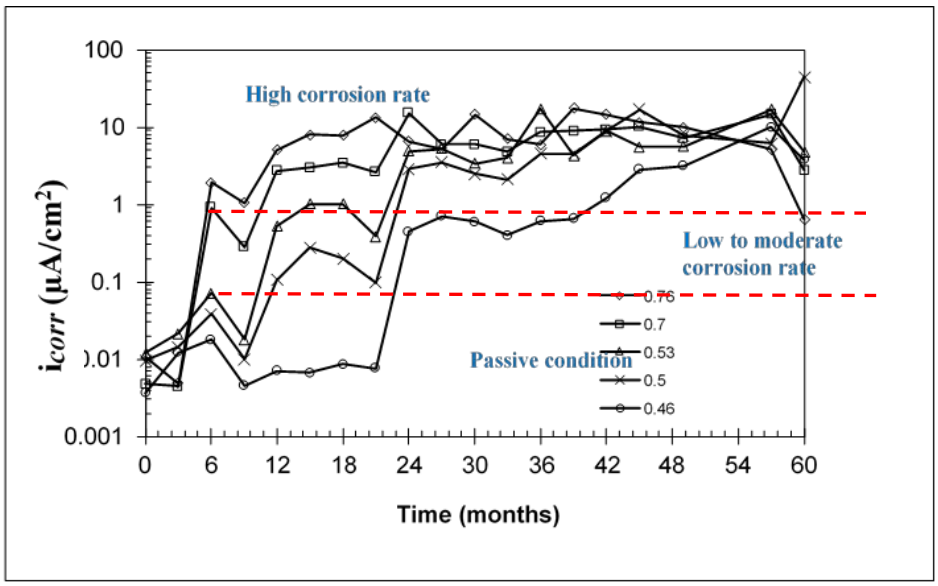

Figure 11. i_{corr} evolution of samples with various *w/c* ratio after 3 days of curing measured for 60 months.

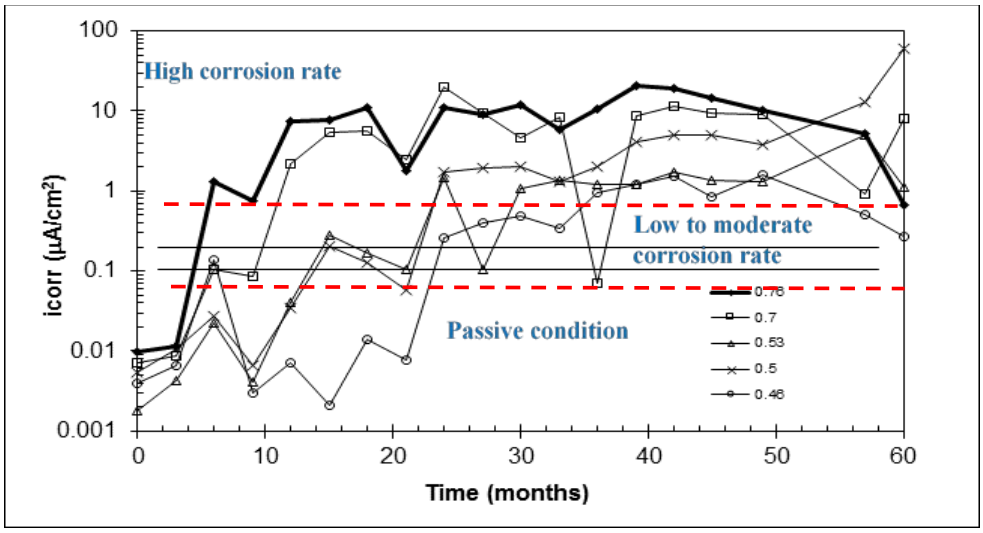

Figure 12. i_{corr} evolution of samples with various *w/c* ratio after 7 days of curing measured for 60 months.

5.1.2. Damage Evolution for Samples Exposed in Galveston, TX Samples

On the USA side of the Gulf of Mexico, the corrosion damage evolution was monitored by EIS testing for almost 17 weeks. With the same sample configuration as the one tested in Mexico, the EIS testing in the USA location (Galveston workstation) was expected to give an alternative insight of how to monitor corrosion kinetics on steel rebar in concrete. The main advantage of EIS is that it can provide more comprehensive information about kinetics on rebar during the exposure compared to direct i_{corr} measurement. The results of EIS spectra are presented in various plots: (1) Nyquist, (2) impedance modulus, and (3) phase angle plots. Figures 14 and 15 represent EIS signal for samples exposed to predominant wings for 0.45 w/c ratio. During the exposure time, we could see the formation of 2 semicircles corresponding to the impedance (or resistance) at the rebar/concrete interface and the resistance of the concrete. The semicircle at low frequencies (in the right position) decreases the diameter with time. This latter considers the degradation of the rebar. The semicircle at high frequencies (left side of the plot) reveals the properties of the concrete with time. Figure 15 shows predominant wings conditions for the same w/c ratio samples. The results show only one time constant or semicircle, this latter represents the behavior of the rebar/concrete interface with time with no explicit demonstration of a passive layer, the impedance magnitudes are lower than no predominant wings exposure. The formation of a stable layer is considered when no predominant wings are facing the samples. The magnitudes of impedance and the mechanistic process (charge and mass transfer) help to understand the rebar damage evolution process with time. The formation of a passive layer considers a mass transport mechanism control during non-predominant wings conditions. While no stable passive layer conditions influence charge transfer process the impedance magnitudes are lower and decreasing faster wit time. Figure 16 and 17 show the same behavior as the previous samples, the predominant wings influence the mechanism with time and the damage evolution of the rebar at deeper position conditions as previous samples. The samples showing 2cm depth have same behavior as the ones with 1.5 cm depth.

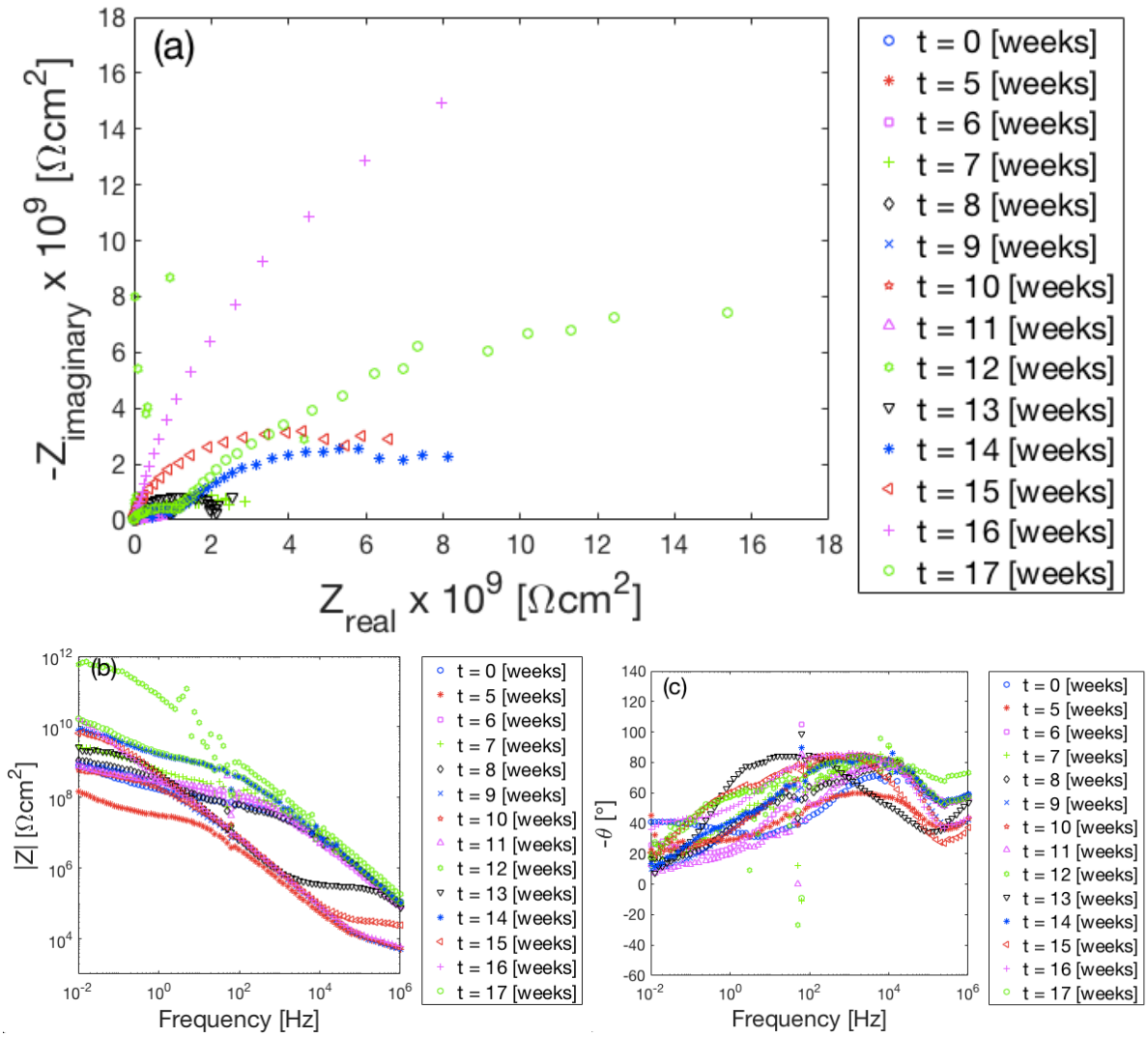

Figure 13. Nyquist (a), Bode (b), and phase angle (c) plots for rebar in concrete with *w/c* of 0.45 at 1.5 cm deep under non-predominant wind.

In general, for all samples, the corrosion kinetics (represented by the size of the semicircle) fluctuated every week during 17 weeks of testing (Figures A-1(a) – A-7(a)). However, all samples show a trend of increased capacitive loops from initial time up to week 17. Another observation in the Nyquist plots is that the charge transfer reactions which are typical corrosion process became less dominant with increasing time. This is evident from the change of curve shape from a semicircle to a slanted line-like curve, which occurs from medium to low frequencies.

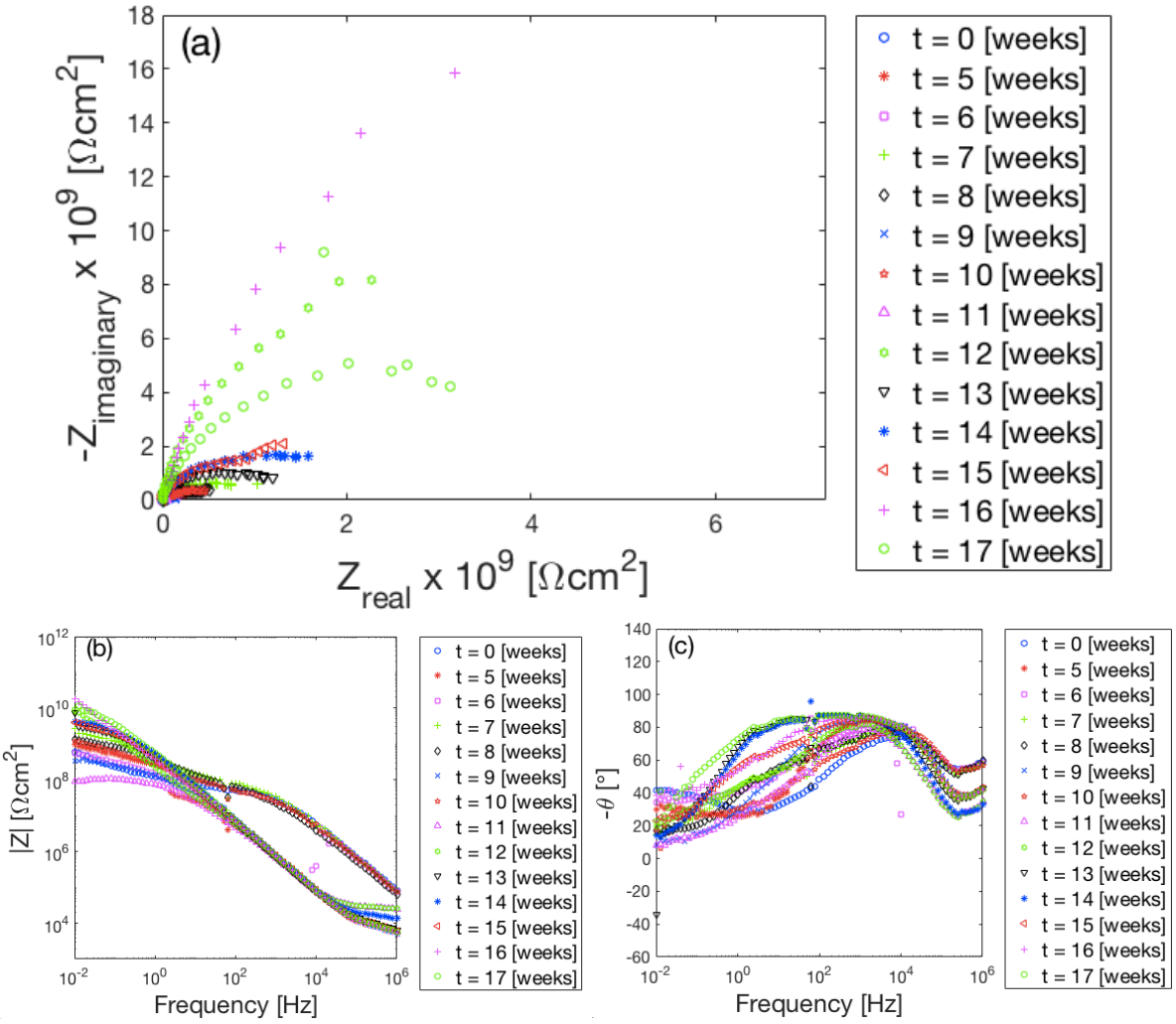

Figure 14. Nyquist (a), Bode (b), and phase angle (c) plots for rebar in concrete with *w/c* of 0.45 at 1.5 cm deep under predominant wind.

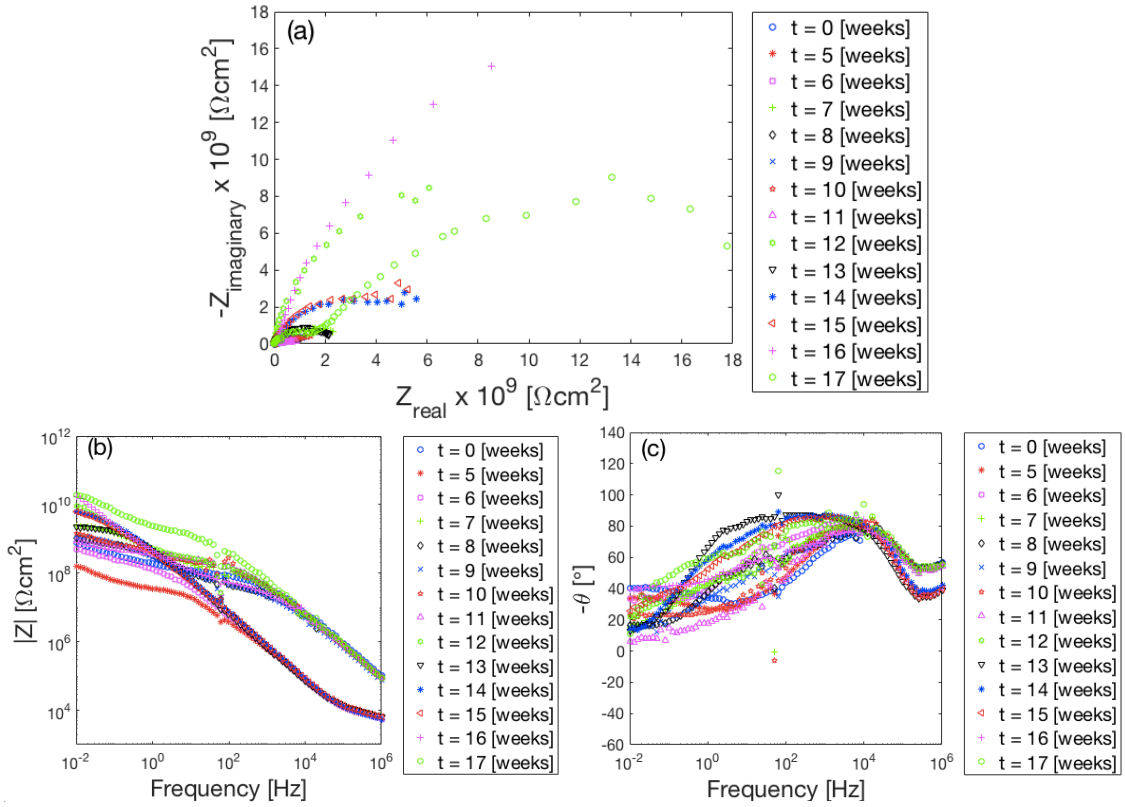

Figure 15. Nyquist (a), Bode (b), and phase angle (c) plots for rebar in concrete with *w/c* of 0.45 at 2 cm deep under non-predominant wind.

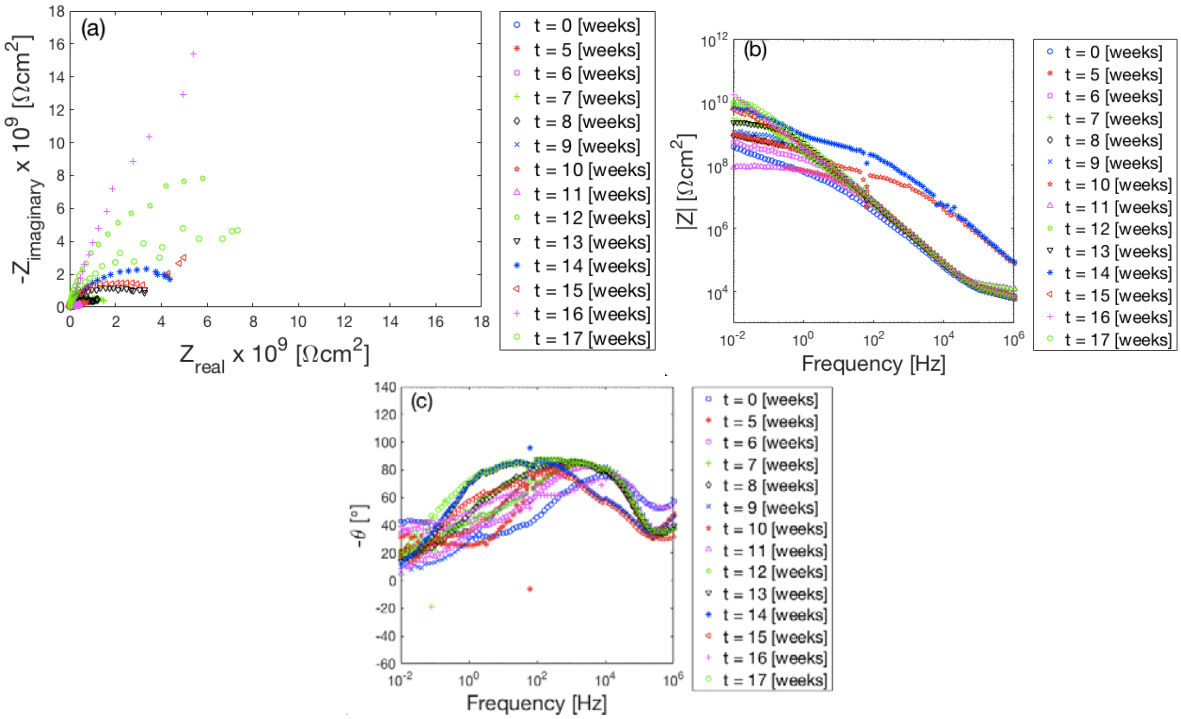

Figure 16. Nyquist (a), Bode (b), and phase angle (c) plots for rebar in concrete with *w/c* of 0.45 at 2 cm deep under predominant wind.

From the impedance modulus plots at the low frequencies (Figures 14-17 and the ones represented in the Appendix), the modulus values initially decrease from around 10^9 to 10^8 ohm.cm^2 from week 0 to 8, indicating that the corrosion rate increased during this period. The horizontal or near-horizontal lines from 100 to 0.01 Hz are indicative of resistive behaviors that are related to charge transfer reactions during the corrosion process. However, from week 8 to 17, in general, the modulus values increased from 10^9 to 10^{10} ohm.cm^2. The horizontal lines that appeared from 100–0.01 Hz from week 0 to 8 gradually disappeared and transformed to slanted lines, which are indicative of capacitive behaviors. In this case, these capacitive behaviors are likely related to a slowdown in corrosion rate due to passive film formation on the rebar. Normally, such an increase in impedance modulus with time for a system that is not protected and exposed to the corrosive environment is not expected. This unexpected increase in impedance modulus with time could be associated with the slower diffusion of chloride compared to oxygen diffusion in the air.

The maximum peak of phase angle plots (Figures 14 – 17 and the ones represented in the Appendix A) increases with time. After around week 15, the maximum peak is located at around 90°, which indicates that the capacitive behaviors of rebars were dominant. These behaviors could be associated with the passive film formation, which slowed down the corrosion kinetics during exposure at Galveston. A thorough observation of the phase angle plots showed that from week 0 to 8, in general, the maximum peak became narrower and shorter (lower degree) with time, indicating an increase in corrosion activation. In contrast, from week 8 to 17, the maximum peak of phase angle plots became wider and taller (higher degree), indicating a transformation from resistive to capacitive behaviors. While the resistive behaviors are related to corrosion activation, the capacitive behaviors are for passivation or corrosion slowdown.

The effect of the position of the samples with predominant wind on corrosion was found to be insignificant in terms of magnitude, as a small change in the impedance modulus was observed when the wind condition was changed from non-predominant wind to predominant at every combination of *w/c* ratio and depth of measurement. Similarly, the influence of depth of measurement on the corrosion process is also unclear. The impedance modulus only changed slightly when the depth was varied from 1.5 to 2.0, and 3.0 cm at every combination of *w/c* ratio and angle. Lastly, the role of *w/c* ratio on corrosion behavior of rebars was also minor. An increase in *w/c* ratio from 0.45 to 0.65 constantly produced similar impedance modulus values.

These insignificant roles of *w/c*, depth of measurement, and wind dominance might be attributed to low diffusion of aggressive anions (e.g., chloride) in concrete exposed to air in Galveston. In the air exposure, the oxygen diffusion is highly correlated to chloride. This situation might help the rebars repaired their passive films. In their passive state, the effect of w/c, depth of measurement, and wind dominance became less obvious.

Although the environment between the Mexico and USA side of the Gulf of Mexico could potentially be considered similar, the variations in the environment are expected to be minor. Therefore, correlating the data from Mexico and USA side might be acceptable. As can be seen from Figures 11–13, from the results in the Mexico location, in less than 17 weeks (4 months)

of testing or exposure, the concrete samples (w/c 0.45) were generally still in the passive condition. This agrees with the EIS results obtained in the USA experiments.

5.2. Probability of Failure Based on Corrosion Assessment

Figure 17 shows the comparison between the actual chloride concentration and our predicted chloride concentration, at various concrete depths. The prediction error, which is the difference between the predicted and actual values, was also calculated and plotted relative to the actual chloride concentration (Figure 18). Those two figures were generated from the results of the statistical model based on the reference case, and the model parameters of Table 3 were used. As an example, the governing equation did not have any correction factors for the different sample conditions by different *w/c* ratios and the length of concrete curing days.

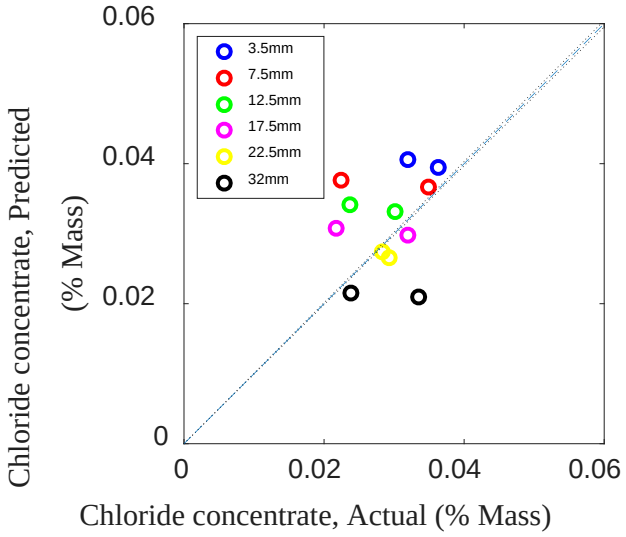

Figure 17. Chloride diffusion, Prediction vs Observation without correction factors.

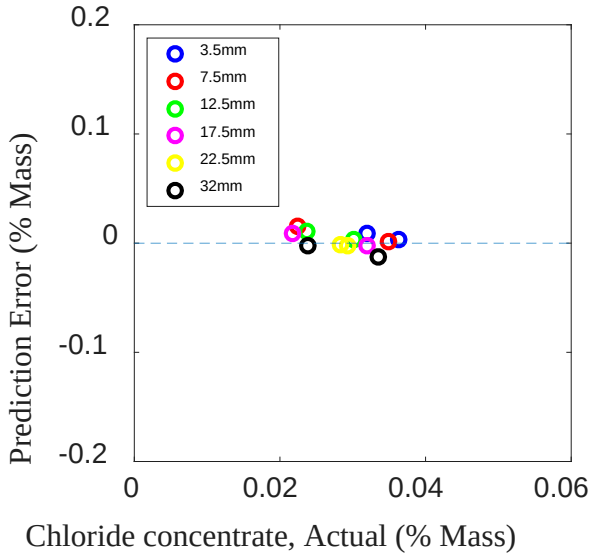

Figure 18. Model prediction error without correction factors.

Figure 19 shows the comparison between the actual chloride concentration and predicted chloride concentration, for varying depths of measurements. The prediction error was also calculated and plotted relative to the actual chloride concentration (Figure 20). Those two Figures were generated from the Bayesian model using the model parameters in Table 3.

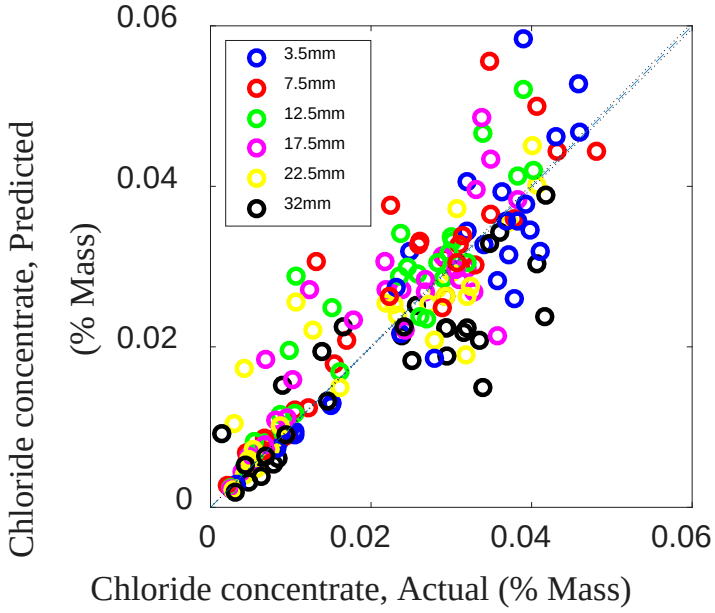

Figure 19. Chloride diffusion: Prediction vs. observation using *w/c* correction factors.

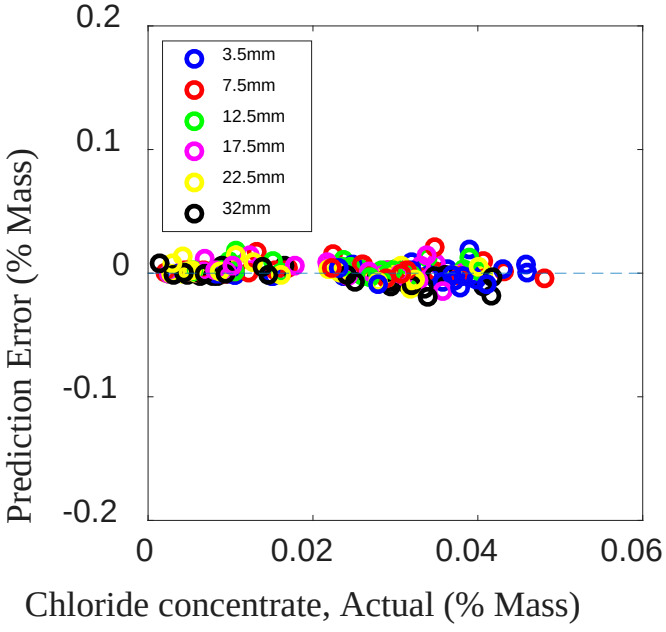

Figure 20. Model prediction error using *w/c* correction factors.

Based on the parameters determined so far, it was possible to estimate the corrosion initiation time for the different *w/c* ratios based on the Model B $T_{corr,B}$ equation, which estimates the time to corrosion initiation using the previously estimated statistical parameters [Equation 7, restated below for reference]. As expected, at the same level of surface chloride concentration, the corrosion was expected to initiate earlier in concrete with higher *w/c* ratios. One exception case that did not follow the general corrosion initiation time trend was *w/c* = 0.46; we suppose that this sample did not cure well, and so it might have had a much higher permeability than the other samples, resulting in a much lower chloride threshold value that triggers corrosion initiation earlier than *w/c* = 0.5 and 0.53 under certain surface chloride concentrations.

$$\text{Model B: } T_{corr,B} = \left[\frac{d_c^2}{4S\alpha_1\theta_1(\theta_2)^{\theta_3}}\left[erf^{-1}\left(1-\frac{C_{cr}}{C_s}\right)\right]^{-2}\right]^{1/1-\theta_3} \qquad [7]$$

The critical surface chloride concentration of each *w/c* ratio was observed to divide each curve into two phases. For example, for the *w/c* = 0.76 or 0.7 cases, the T_{corr}/C_s value changes significantly around the surface concentrations of 0.08 or 0.09, respectively. Therefore, the surface concentration lower than the critical value showed a much longer average time period for corrosion initiation, even with the much greater changing rate compared to the case of the surface concentration exceeding 0.07. There was also a trend of this critical surface chloride concentration throughout the *w/c* ratio, which was also generally increased with it, and such this trend is consistent with the trend between T_{corr} and *w/c* ratio.

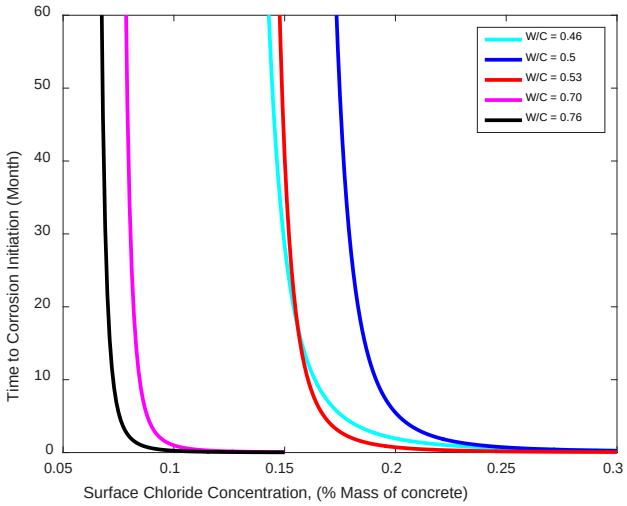

Figure 21. T_{corr} values for different surface chloride concentration.

The reliability of the achieved T_{corr} values could be quantified by suggesting the reliability index or the failure probability. The reliability index is an indicator that shows the reliability of the model, and it is used to calculate the failure probability of the estimation of the performance of interest, T_{corr}. The reliability index is the ratio of the mean and the standard deviation of the T_{corr}. The failure probability is the possibility of the wrong estimation, and it is calculated using the cumulative distribution of the reliability index. Both the reliability index and the failure probability were evaluated based on the FORM, considering the previously estimated T_{corr} values.

Figures 23 to 27 show the failure probability of concrete structures with different *w/c* ratios and chloride surface concentrations. All the plots express the reliability of the T_{corr} estimation over time, and it was set that all cases have a similar T_{corr} value within their surface concentration range. The higher the w/c and concentration of surface chlorides the shorter the time to reach the failure mode, the plots shows the trend the probability of failure with time. We can see Figure 23(w/c=0.46) reaches 100% failure probability at longer times (more than 15 years) for all chloride surface concentrations with respect to higher w/c=0.76. The time to reach 100% probability of failure was less than 8 years for all surface chloride concentrations.

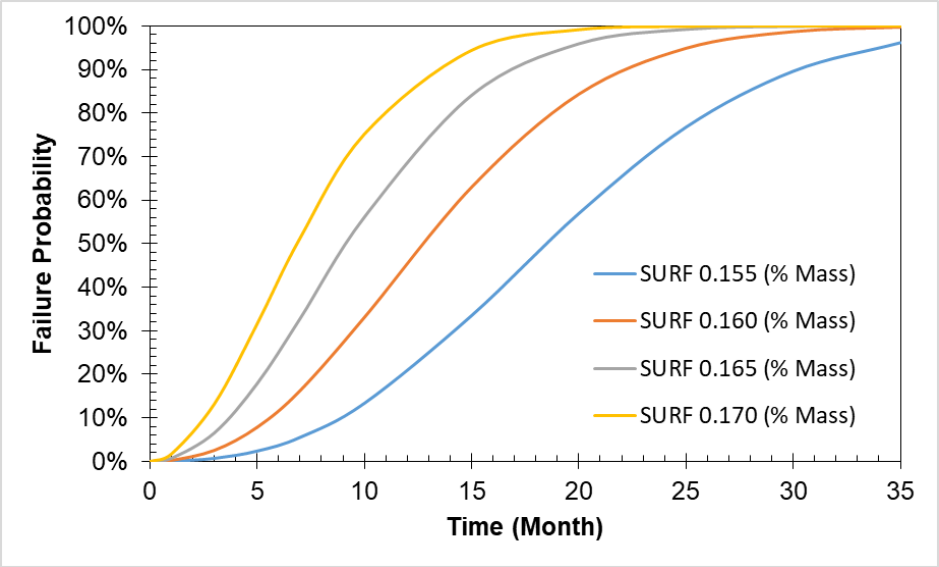

Figure 22. Failure probability analysis for *w/c* = 0.46 with various surface concentrations.

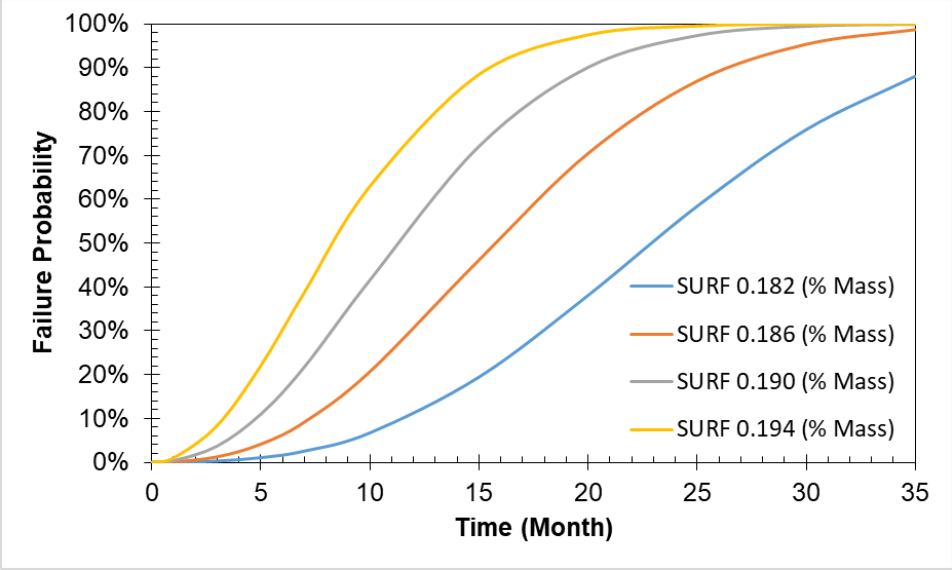

Figure 23. Failure probability analysis for *w/c* = 0.50 with various surface concentrations.

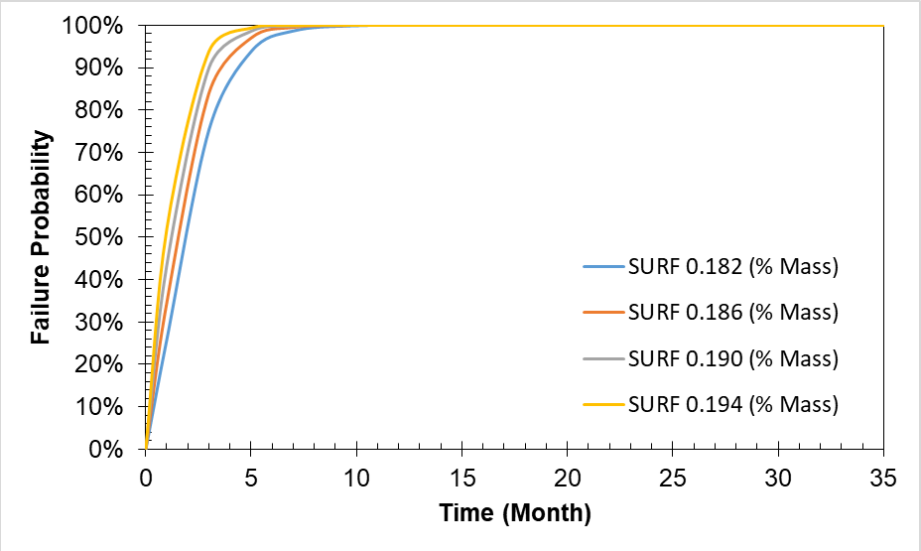

Figure 24. Failure probability analysis for *w/c* = 0.53 with various surface concentrations.

It was observed that the failure probability increases with time because of the decrease of the reliability index. For the lower surface concentration with relatively higher T_{corr} value, the failure probability experienced a slower increase of its value compared to the case with higher surface concentration. For both figures, there was a trend that the higher surface concentration triggers the earlier corrosion initiation, therefore, the reliability of the T_{corr} estimation decreases faster over time because such a case exceeds the T_{corr} value earlier than the lower surface concentration case.

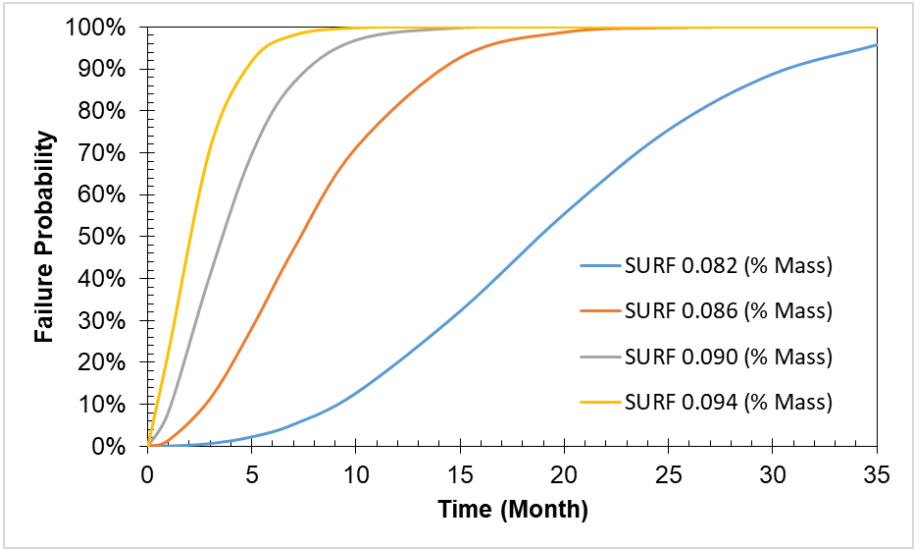

Figure 25. Failure probability analysis for *w/c* = 0.70 with various surface concentrations.

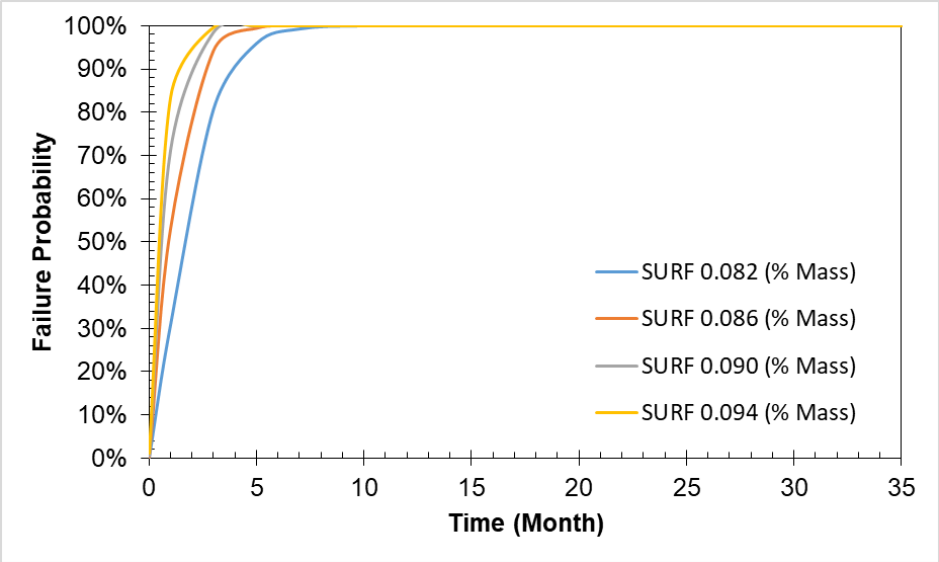

Figure 26. Failure probability analysis for *w/c* = 0.76 with various surface concentrations.

Additionally, at the same surface concentration range, it was estimated that the concrete with higher *w/c* ratio experience earlier corrosion initiation, as it is likely to have a higher chloride diffusivity value that triggers faster chloride ion transport. For the same surface chloride concentrations, increasing the *w/c* ratio results in higher failure probability. For example, for concretes with *w/c* ratios = 0.50 and 0.53, at the surface chloride concentration of 0.182%, 50% failure probability in a lower *w/c* ratio (0.50) happens almost 10 times slower than the higher *w/c* ratio (0.53). As can be seen in Figure 20 and 21, 50% failure probability in the concrete with a *w/c* ratio of 0.53 occurs after 25 months, while the concrete with a lower *w/c* ratio happens after 2 months.

Figures 28 to 31 show the 3-D relationship among the surface chloride concentration, period, and failure probability for various *w/c* ratios. From these Figures, it is possible to observe the increasing speed of failure probability over time for different surface concentrations through estimating the slope of the surface. The reason for the similar shape for each plot is that the surface concentration range was set to have similar T_{corr} values. Under the same high surface concentration for all *w/c* cases, it was observed that the failure probability starts from higher points, then reached 100% over time.

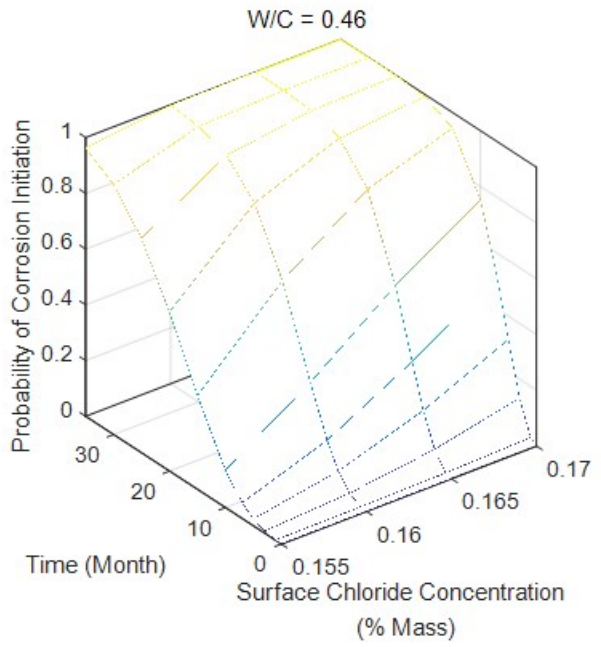

Figure 27. The relationship among surface concentration, time, and failure probability at *w/c* = 0.46.

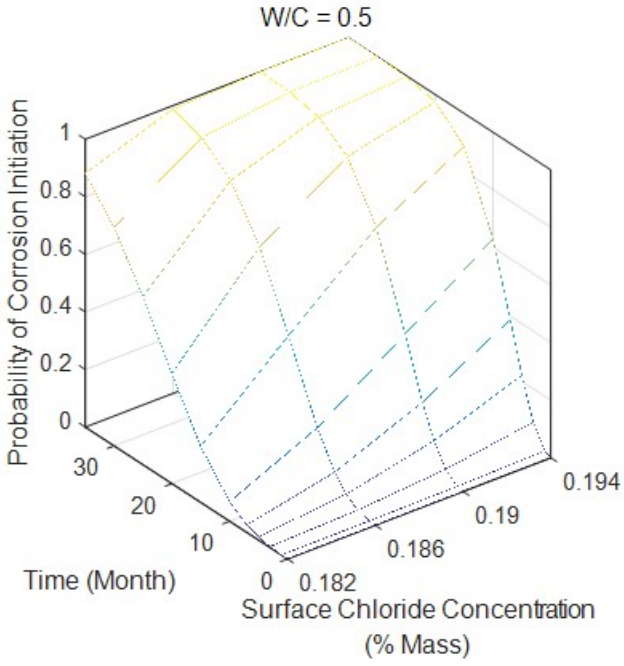

Figure 28. The relationship among surface concentration, time, and failure probability at *w/c* = 0.50.

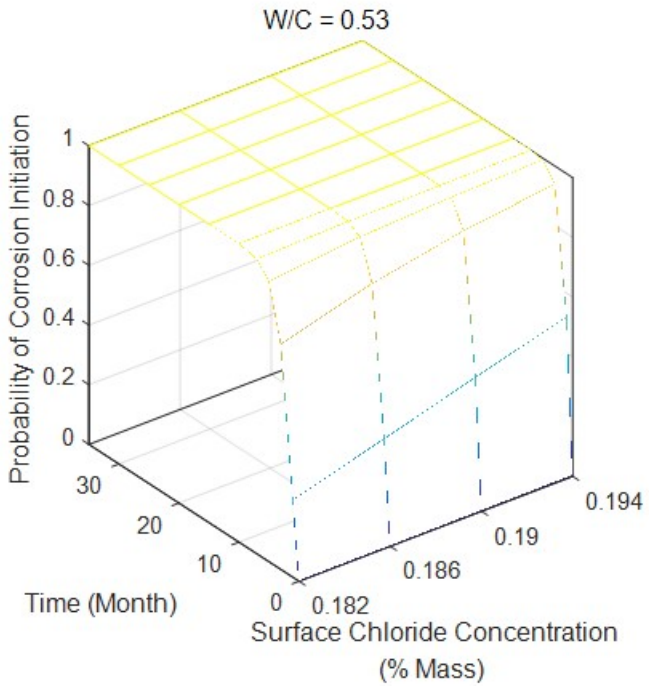

Figure 29. The relationship among surface concentration, time, and failure probability at *w/c* = 0.53.

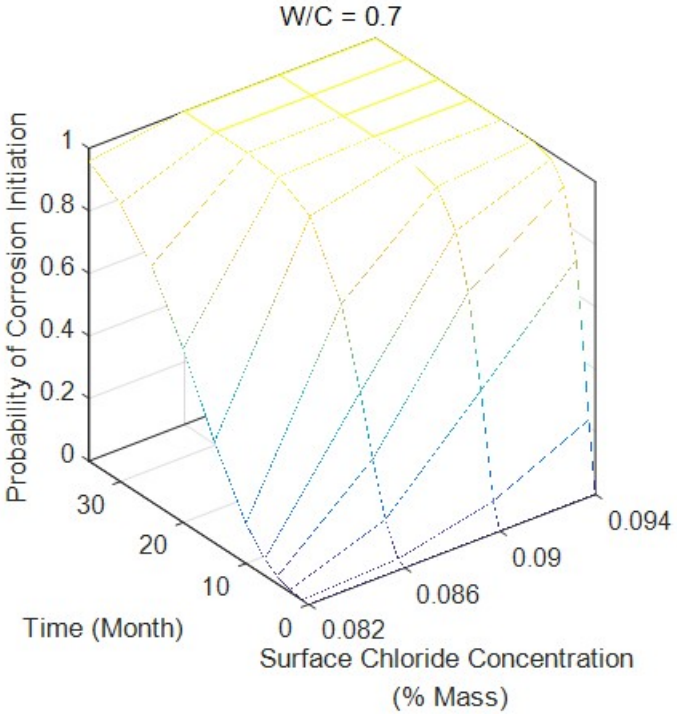

Figure 30. The relationship among surface concentration, time, and failure probability at *w/c* = 0.70.

5.3. Service Life Prediction

5.3.1. Based Service Life Prediction Model

The samples exposed to off-shore environment did not have any load, the service prediction model includes loading conditions, we estimate the service life based on the limit state function and using a probabilistic formulation embracing independent random variables to estimate the prediction of occurring flexural failure of a concrete beam. The statistical characteristics (mean value or bias, COV, and distribution type) of the random variables can be determined experimentally for the parameters investigated in this study or from the literature (e.g., Ghanooni-Bagha *(23)*, Nowak and Collins *(18)*, Okeil et al. *(24)*). The structural reliability problem can be solved using various methods, such as Monte Carlo simulations (MCS) and FORM. In this study, FORM was used for its superiority to MCS, which requires additional computing resources, especially for solving the problem over an extended design life of the structure. The metallic structure used to demonstrate the proposed framework is simply-supported RC metallic structure subjected to uniformly distributed dead and live loads. For the calculation we assume a metallic structure span length is 10 m long with a rectangular cross-section (0.35 m wide and 0.80 m high). The tensile reinforcement is placed in two rows. The first row, A_{s1}, has nine rebars of 0.0254-m diameter ($A_{s1} = 0.00456\ m^2$), while the second, A_{s2}, has three rebars of 0.043-m diameter ($A_{s2} = 0.004356\ m^2$). Each random variable with means, coefficients of variation, and distribution type are defined in Tables 6 and 7.

Table 6. Statistical characteristics of ambiguous variables within model.

Parameter	Mean	COV	Distribution
ξ_M	1.1	0.120	Normal
K	0.59	0.05	Normal
α	0.5	0.12	Log-Normal

Table 7. Statistical characteristics of mechanical features within model.

Parameter	Mean	COV	Distribution
f'_c	27.6 MPa	0.18	Log-normal
f_y	414 MPa	0.10	Log-normal
Dead Load	1.05*$M_{n,D}$	0.10	Normal
Live Load	0.3*$M_{n,L}$	0.6	Normal
d_1 (effective depth for A_{s1})	0.70 m	0.01	Normal
d_2 (effective depth for A_{s2})	0.625 m	0.01	Normal
Concrete cover	0.09 m	0.12	Normal

5.3.2. Application of Reliability-Based Service Life Prediction Model

Here, we demonstrate how the probabilistic framework could be used in decision-making for repair and maintenance operations of bridge structures prone to corrosion. A sample of RC beams subjected to corrosion was analyzed using the methodology described above. FORM was used to calculate the reliability index, β, of the considered beam over time using the corrosion rate from Eq. (19) and the limit state function from Equation 17. As corrosion ensues, the area of steel reinforcement drops following Eq. (21) and the steel yield stress changes following Equation 18. These two parameters are the main parameters that affect the tensile force achievable in any RC beam; hence the cross section's flexural resistance drops, and its

structural reliability starts decreasing over time, assuming that the load demands are stationary. Figure 31 shows the results for how β varies over a typical design life of 75 years.

$$i_{corr}(\mathrm{t}) = \frac{37.8(1-w/c)^{1.64}}{C} \quad [20]$$

in which, w/c = the water to cement ratio for the concrete mix used in pouring the studied beam. A value of 0.4 is assumed in this work. The corrosion rate term is modified to allow for corrosion rates at the beginning of corrosion initiation, $i_{corr}(t)$, as well as time after the corrosion initiation process.

$$i_{corr}(t) = \begin{cases} i_{corr}(1) & 0 \le t \le 1\ year \\ 0.85 i_{corr}(1)\ t^{-0.29} & t > 1\ year \end{cases} \quad [21]$$

Pitting corrosion is not considered in this paper (only general or uniform corrosions are considered). Using Faraday's loss of electrochemical equivalence, the reduction in diameter, ΔD (m), over time is noted below

$$\Delta D(t) = 0.0232 i_{corr}(t) \quad [22]$$

As the diameter of the reinforcement is decreased, the area also decreases proportionally.

$$A_s(t) = n\frac{\pi[D_0 - \Delta D(t)]^2}{4} \ge 0 \quad [23]$$

Three degradation scenarios are presented, each corresponding to a different corrosion rate. Regarding corrosion, they can be thought of as different cases of exposure conditions (aggressive, moderate, and minimal) or variations of the quality of the product. It can be seen that β starts at an almost constant value for the initial few years, until the onset of corrosion. The capacity degradation is then reflected into lower β values; thereafter depending on the specific conditions of the beam. This plot can be used by infrastructure owners to estimate the remaining service life of a structure. To determine the remaining service life, t_i, an acceptable reliability index, $\beta_{\text{threshold}}$, must first be set. Design provisions in most modern design codes *(15)* are calibrated for a target reliability index, β_{target}, which is equal to 3.5. However, for infrastructure management, owners might allow lower β values for various reasons, such as reflecting the load posting of the bridge. In Figure 32, for a specific $\beta_{\text{threshold}}$, the acceptable service life of the structure can be easily determined from the intercept of this threshold with each of the three curves, representing different degradation scenarios, $t_{i,1}$, $t_{i,2}$, and $t_{i,3}$. It can be seen that all scenarios yield a service life less than the typical 75 years design life targeted by most modern design codes. Infrastructure replacement is not always a feasible alternative because of limited resources. Hence, rehabilitation is often the chosen solution.

Figure demonstrates another aspect of the how the proposed framework can be used to choose between rehabilitation alternatives. The most aggressive scenario is used in this case, with three alternative assumed repair methods. The goal of any repair method is to ensure the structural integrity of the structure under normal operating conditions. Two repair alternatives, Repair #1 and Repair #2, restore the reliability index to its initial value before the onset of

corrosion. The difference between these two methods is that Repair #1 does little to reduce the rate of corrosion, which results in a service life of slightly over 50 years. Conversely, Repair #2 slows the degradation rate, which results in a service life of about 60 years. Reducing the degradation rate can be achieved using different methods. For example, Fiber Reinforced Polymer wrapping of RC beams is known to deprive the corrosion cell of oxygen, which results in slower corrosion rates. Nevertheless, the achieved service is still below what an owner might desire (e.g., 75 years). To achieve a longer design life, Figure 32 shows that a higher initial reliability index, β, will be needed for the same corrosion rate as that resulting from Repair #2. This is the case for Repair #3, for which the initial β after repair is increased, which adds about 5 years of service life over Repair #2 alternative.

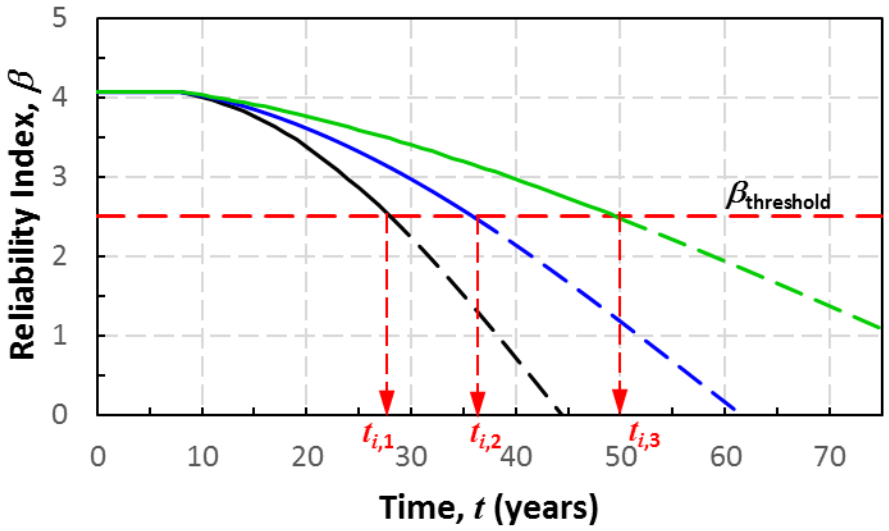

Figure 31. Reliability index vs. time.

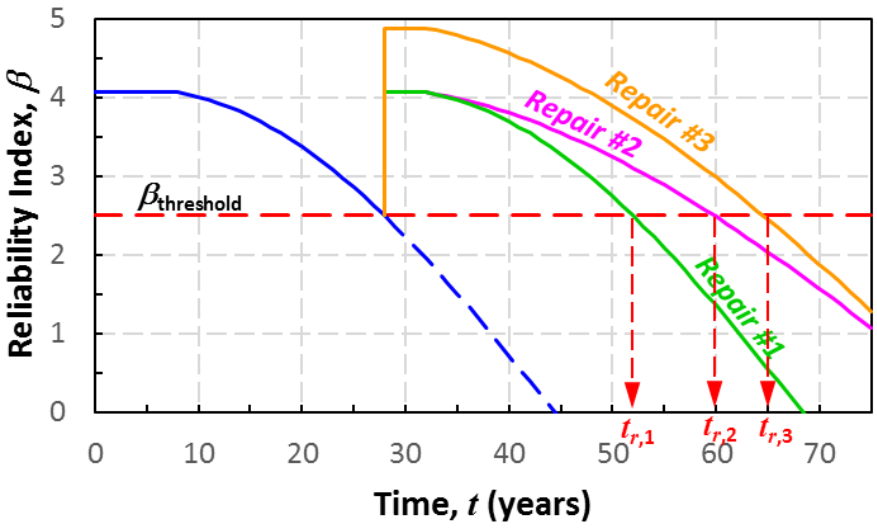

Figure 32. Effect of different intervention strategies on expected service life.

5.4. Reliability-Based Framework

The proposed framework is based on a series of steps taken to make important decisions for repairing, inspecting and maintaining reinforced concrete assets and by considering the development in this work. The steps include:

Review Inspection Capabilities: This step follows the technologies available to measure corrosion rates or characterize corrosion. The two technologies used on this work includes electrochemical methods and guard ring technology. Nondestructive evaluation is also other possibility as some examples in Table 8.

Table 8. Some examples of evaluation of NDE technologies.

NDE Techniques	Applications	Limitations
Gecor (polarization technique)	• rebar corrosion rate • reliability of the structure based on metallic degradation	• Might be difficult to read a rebar network • hard to use in difficult access areas
ER (Electrical Resistivity)	• characterize concrete's susceptibility to corrosion • resistivity surveys can be used to detect corrosion cells in tandem with another corrosion technique	• the data result is hard to interpretation • automated measurement systems are not currently available • the surface of a test object has to be pre-wetted

In Depth Corrosion Assessment: Following the measurement, the results should be characterized and evaluated based on the parameters considered for the inspection. Corrosion rate, rebar thickness and/or physical characteristics of the rebar among others. Rebar damage evolution is a degradation process with different stages, the corrosion assessment can help to quantify the current status of the rebar by considering different stages.

Bridge Conditions Rating based on Corrosion (Corrosion Susceptibility Index): Corrosion index can be defined based on the degradation mechanism, the index considers the intact stage (or passive) to be the minimum number in a selected scale, i.e. zero to be the intact state. The corroded rebar can be defined as the number five. From the corrosion activation, the following degradation level could be the corrosion rate or wall loss thickness. The index can be expanded from number 5 to number 10, being the latter the most severe corrosion rate or highest wall loss. The numbers in between are qualitative based on the physical parameter of the rebar. Also, the scale can be normalized to be between zero and one.

Preliminary Summary of Repair and Corrosion Control Methods: There are different repair methods for reinforced concrete structures reported previously *(25)*. Following a specific index or number, the repair method used can be correlated with the proposed index. We give an example of used repair methods and corrosion control methods in Table 9. One way of classifying the repair methods, according to Yehia et al. *(26)* could be categorizing them in two different categories: protective methods (e.g., grouting, sealing, overlay, injection) and the second classification is non-protective methods (e.g., overlay, patching, sealing).

Table 9. Repair and corrosion control methods.

Repair Principle	Repair name	Description	Comment
Physical	Patching	• epoxy injection • flood with corrosion inhibitor • surface application of corrosion inhibitor • recoating exposed steel • patching with admixed corrosion inhibitors • combine the methods	• the designer's responsibility to evaluate the repair areas and determine the most suitable repair method; • a cheap way to repair local damage; • not completely waterproof. It may be a temporary remedy to the problem, but it may further deteriorate the problem
Electrochemical	Cathodic Protection	• achieved by supplying an external source of current to counteract the internal corrosion current • can be applied to new construction and rehabilitation	• FHWA has stated that cathodic protection is the only rehabilitation technique that has proven to stop corrosion in salt-contaminated bridge decks regardless of

Expert System for Repair Method and Control Method (Repair Database): When a structure reaches such a degree of deterioration that an intervention and repair decision must be made, it is then necessary to analyze and select the various repair options available. Decision can be based on the requirements (Rq) of the repair material or repaired structure either existed or new design, which are quantified by performance indicators (Ind). The performance indicators could include safety, serviceability and functionality, durability, integrity, and economy. These performance indicators could be defined depending on the element to be characterized. The important of each performance indictor is based on qualitative approach due to the judgment of the person in charge of the structure.

Both parameters, indicators and requirements are defined according with the concrete structure, we can use such parameters in a semi-empirical expression as follows:

$$Req = \frac{\sum Ind}{number\ of\ Ind} \qquad [24]$$

A final assessment could consider a repair (in nature) index QI, which can be defined based on all Requirements. In addition, a weigh factor due to the level of importance that defines the index. This decision step can be complemented with practical or historical parameters (included in the weight factor) of a defined concrete structure.

Remaining Life Models based on Reliability: By following the proposed computational framework, our Bayesian-based model can be updated, improved and modified using datasets that become available in the future. In the second model, the FORM is used to analyze the structural reliability problem. Both models show how this framework can be used to help infrastructure owners make maintenance and repair decisions to achieve their goals (e.g., extended service life). The models cited in the proposed methodology for the reliability framework achieve one of the main goals of this work; to estimate the structural degradation of RC structures and infrastructures based on degradation mechanisms and monitoring tools for corrosion. Finally, the experimental data obtained by electrochemical methods helped us to understand the initiation mechanisms in detail at the micro-interface level and support both models in terms of fundamentals of degradation and potential control actions.

Figure 32 demonstrated how the proposed framework can be used to choose between rehabilitation alternatives and form a continuous optimization cycle (see Figure 33). The goal of any repair method is to ensure the structural integrity of the structure under normal operating conditions. Two repair alternatives, Repair #1 and Repair #2, restore the reliability index to its initial value before the onset of corrosion. The difference between these two methods is that Repair #1 does little to reduce the rate of corrosion, which results in a service life of slightly over 50 years. Conversely, Repair #2 slows the degradation rate, which results in a service life of about 60 years. Reducing the degradation rate can be achieved using different methods. For example, Fiber Reinforced Polymer wrapping of RC beams is known to deprive the corrosion cell of oxygen, which results in slower corrosion rates. Nevertheless, the achieved service is still below what an owner might desire (e.g., 75 years). To achieve a longer design life, Figure 33 shows that a higher initial reliability index, β, will be needed for the same corrosion rate as that resulting from Repair #2. This is the case for Repair #3, for which the initial β after repair is increased, which adds about 5 years of service life over Repair #2 alternative.

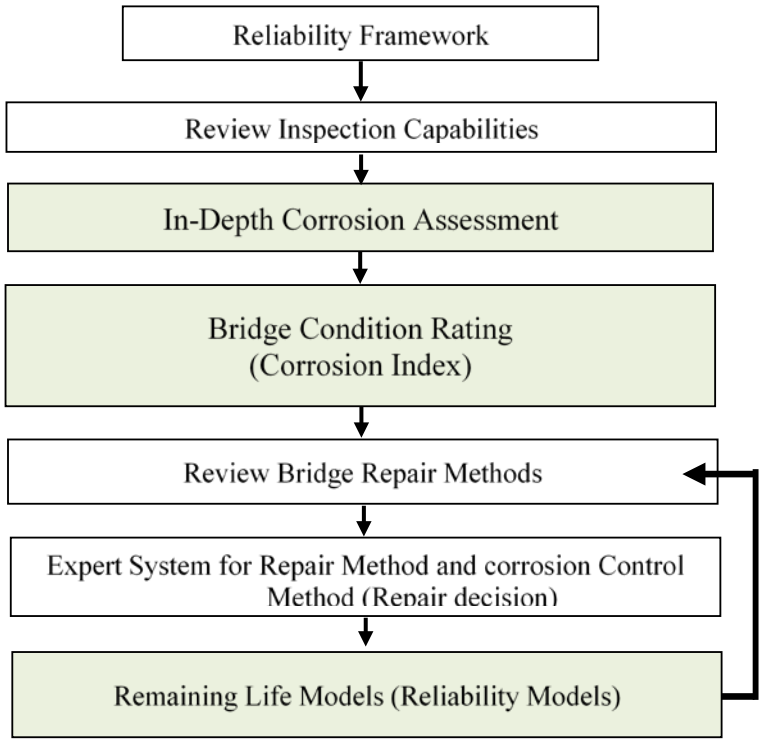

Figure 33. Steps for different intervention strategies on expected service life (green-colored steps developed in this project).

6. CONCLUSIONS

1. For the EIS measurement in Galveston (USA side), corrosion kinetics in concrete structures tested in the seacoast exposure became faster with time during the first 8 weeks of exposure. This is evidenced by a decrease of the impedance modulus from around 10^9 ohm.cm^2 at week 0 to 10^8 ohm.cm^2 at week 8. In contrast, from week 8 to 17, the modulus values increased from 10^9 to 10^{10} ohm.com^2, indicating a slowdown in the corrosion rate. This is also supported by the Nyquist plots, which show a transition from a semicircle to near-slanted line plots (indicative of capacitive behavior) from week 8 to 17. The maximum of the phase angle peak became wider and higher (in terms of the degree) when comparing weeks 8 to 17 to weeks 0 to 8, which suggested the transition from the resistive to capacitive behaviors.
2. The role of w/c, curing time, and wind dominance in the corrosion kinetics was not clearly observed in the EIS spectra measured in Galveston. Regarding corrosion, the mechanistic analysis can be used to support the use of electrochemical techniques for the reliability framework.
3. For the corrosion rate (represented by corrosion current densities) measurements in the Mexico location, the results clearly showed that the corrosion rate increased with increasing the w/c ratio and time. This difference in corrosion behaviors for samples tested on the USA and Mexico sides of the Gulf of Mexico might be attributed to differences in the rainfalls in these areas during the measurement periods. Our methodology will follow the steps in the framework for reliability; the technology can be implemented for inspection routines.
4. In this study, a reliability-based framework that incorporates the developed mathematical corrosion model for prediction of RC beams service life was developed. The model accounts for uncertainties in both corrosion degradation and structural performance. The FORM is used to analyze the structural reliability problem. Results from the developed model show how this framework can be used to help infrastructure owners make maintenance and repair decisions. In particular, it was demonstrated how our framework could be used to (a) predict the service life that meets a given performance level, and (b) assist in selecting repair intervention strategies to extend the structure's service life. Due to the flexibility of new data or existing corrosion-related data, the model is also part of the proposed framework.
5. Based on our preliminary mathematical modeling, we found that the technology implemented for corrosion rate in-situ and real-time measurements follow the requirements for the proposed framework. Electrochemical testing is also capable of supporting the different stages of the repairing and inspection actions.
6. The preliminary framework is based on corrosion assessment by considering the main threat. A flow diagram is proposed to follow up with the implementation and further research in this topic. The proposed framework can be converted in a procedure o methodology.

7. RECOMMENDATIONS

For future research:

1. EIS measurement and i_{corr} at the USA side are performed when the concrete structures become electrochemically active. The results of this measurement can be used as the inputs for the mathematical modelling for the USA side.
2. New corrosion model will be calibrated for coastal areas in the southern United States and its results will be compared to different corrosion models from the literature. The effects of different parameters on the decision making will be assessed using the best performing calibrated corrosion model. The included parameters will be a wider design space (e.g. different beam geometries and reinforcement details), material properties (e.g., concrete strength and *w/c* ratio), and environmental conditions (e.g., distance from shoreline).

REFERENCES

1. K. Tuutti, Corrosion of steel in concrete, (1982).

2. H. Böhni, Corrosion in Reinforced Concrete Structures, Elsevier, 2005.

3. Otieno M, Beushausen H, Alexander M. Chloride-induced corrosion of steel in cracked concrete – Part I: Experimental studies under accelerated and natural marine environments. Cement and Concrete Research. 2016;79:373-85.

4. Farsani AM, Keshtegar B. Reliability Analysis of Corroded Reinforced Concrete Beams Using Enhanced HL-RF Method. Civil Engineering Infrastructures Journal. 2015;48(2):297-304.

5. L. Tang, Chloride Transport in Concrete - Measurement and Prediction, Research.chalmers.se. (1996). https://research.chalmers.se/publication/1267 (accessed July 12, 2018)

6. B.H. Oh, S.Y. Jang, Y.S. Shin, Experimental investigation of the threshold chloride concentration for corrosion initiation in reinforced concrete structures, Mag. Concr. Res. 55 (2003) 117–124.

7. K.Y. Ann, J.H. Ahn, J.S. Ryou, The importance of chloride content at the concrete surface in assessing the time to corrosion of steel in concrete structures, Constr. Build. Mater. 23 (2009) 239–245. doi:10.1016/j.conbuildmat.2007.12.014

8. P. Arora, B.N. Popov, B. Haran, M. Ramasubramanian, S. Popova, R.E. White, Corrosion initiation time of steel reinforcement in a chloride environment—A one dimensional solution, Corros. Sci. 39 (1997) 739–759. doi:10.1016/S0010-938X(96)00163-1.

9. D.V. Val, P.A. Trapper, Probabilistic evaluation of initiation time of chloride-induced corrosion, Reliab. Eng. Syst. Saf. 93 (2008) 364–372. doi:10.1016/j.ress.2006.12.010.

10. E. Bastidas-Arteaga, A. Chateauneuf, M. Sánchez-Silva, P. Bressolette, F. Schoefs, A comprehensive probabilistic model of chloride ingress in unsaturated concrete, Eng. Struct. 33 (2011) 720–730. doi:10.1016/j.engstruct.2010.11.008.

11. Durability of Building Materials and Components 8. (1999) Edited by M.A. Lacasse and D.J. Vanier. Institute for Research in Construction, Ottawa ON, K1A 0R6, Canada, pp. 1343-1356. T. SIEMES, DURACRETE: SERVICE LIFE DESIGN FOR CONCRETE STRUCTURES, A basis for durability of other building materials and components?.

12. P. Castro-Borges, M. Balancán-Zapata, A. López-González, Analysis of Tools to Evaluate Chloride Threshold for Corrosion Onset of Reinforced Concrete in Tropical Marine Environment of Yucatán, México, J. Chem. 2013 (2013) 1–8. doi:10.1155/2013/208619.

13. P. Castro-Borges, M. Balancán Zapata, A. López González, “Analysis of tools to evaluate chloride threshold for corrosion onset of reinforced concrete in tropical marine environment of Yucatán, México”, Journal of Chemistry, Vol 2013, Article ID 208619, 8 p, 2013, FI JCR 0.5 en 2011.

14. P. Castro-Borges, L. Veleva, M- Balancán –Zapata, J. M. Mendoza-Rangel, L. A. Juárez, "Effect of environmental changes on chemical and electrochemical parameters in reinforced concrete. The case of a tropical marine atmosphere", Int J Electrochem Sci, Vol 8, Mayo 2013, pp. 6204-6211 , ISSN 1452-3981, FI JCR 3.7 (2011)15. American Association of State HT, Officials. AASHTO LRFD bridge design specifications, seventh edition, 2014, U.S. customary units : 2015 interim revisions2014.

15 P. Castro, O.T. De Rincon, E.J. Pazini, Interpretation of chloride profiles from concrete exposed to tropical marine environments, Cem. Concr. Res. 31 (2001) 529–537. doi:10.1016/S0008-8846(01)00453-7.

16. Zivica V. Corrosion of reinforcement induced by environment containing chloride and carbon dioxide. Bulletin of Materials Science. 2003;26(6):605-8.

17. Bastidas-Arteaga E, Soubra A-H. Reliability Analysis Methods. Stochastic Analysis Modelling: ALERT Doctoral School 2014; 2014.

18. Nowak AS, Collins KR. Reliability of Structures: McGraw Hill, USA; 2000.

19. El-Tawil S, Okeil AM. LRFD Flexural Provisions for Prestressed Concrete Bridge Girders Strengthened with Carbon Fiber-Reinforced Polymer Laminates. Structural Journal. 2002;99(2):181-90.

20. Okeil AM, El-Tawil S, Shahawy M. Flexural Reliability of Reinforced Concrete Bridge Girders Strengthened with Carbon Fiber-Reinforced Polymer Laminates. Journal of Bridge Engineering. 2002;7(5):290-9.

21. Okeil AM, Belarbi A, Kuchma DA. Reliability Assessment of FRP-Strengthened Concrete Bridge Girders in Shear. Journal of Composites for Construction. 2013;17(1):91-100.

22. American Association of State HT, Officials. AASHTO LRFD bridge design specifications, seventh edition, 2014, U.S. customary units : 2015 interim revisions2014.

23. Ghanooni-Bagha M, Shayanfar MA, Reza-Zadeh O, Zabihi-Samani M. The effect of materials on the reliability of reinforced concrete beams in normal and intense corrosions. Eksploatacja i Niezawodnosc – Maintenance and Reliability 017;19(3):393-402.

24. T. Onore, Okeil AM, H. Castaneda, M.R. Taha, A Framework for Reliability Assessment of Corrosion Damaged Reinforced Concrete Structures, proceedings of the 2018 World *Transport Convention Beijing, China, June 18-21, 2018*

25. Sohanghpurwala, A. A. (2006). "Manual on Service Life of Corrosion-Damaged Reinforced Concrete Bridge Superstructure Elements." NCHRP Report 558.

26. Yehia, S., Abudayyeh, O., Fazal, I. and Randolph, D. (2008). "A decision support system for concrete bridge deck maintenance", Advances in Engineering Software, 39, p202-210.

APPENDIX A: EIS EXPERIMENTAL RESULTS FOR REINFORCED CONCRETE SPECIMENS

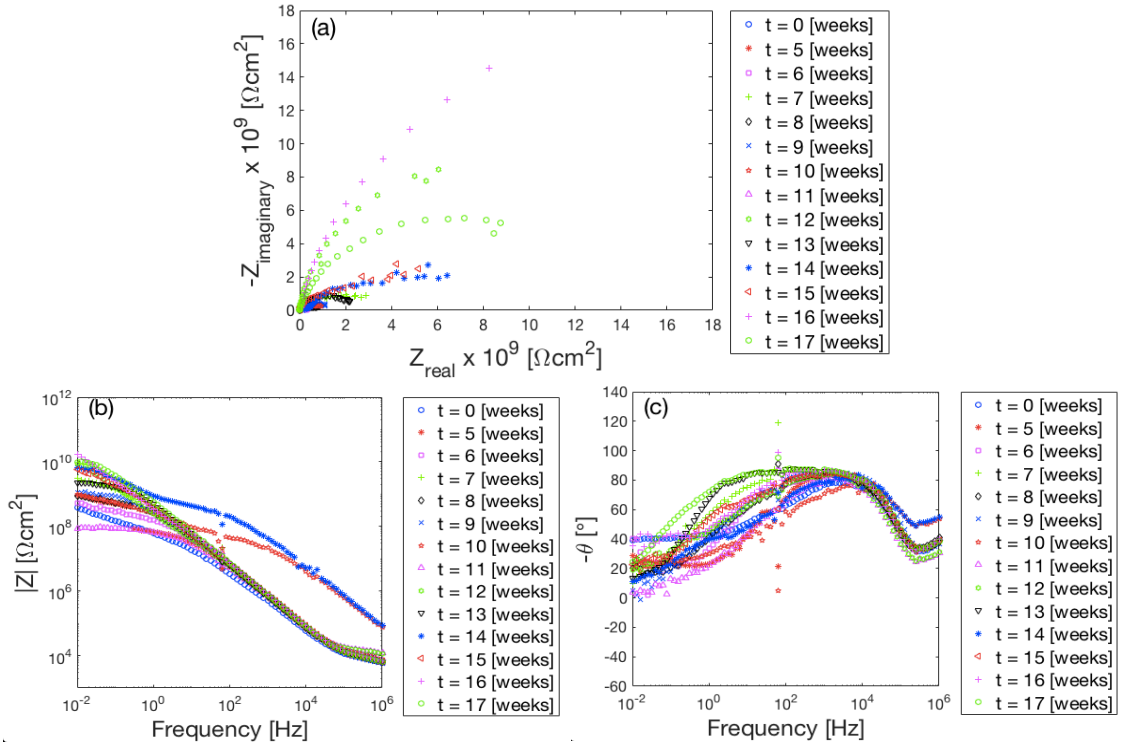

Figure A-1. Nyquist (a), Bode (b), and phase angle (c) plots for rebar in concrete with *w/c* of 0.45 at 3 cm deep under non-predominant wind.

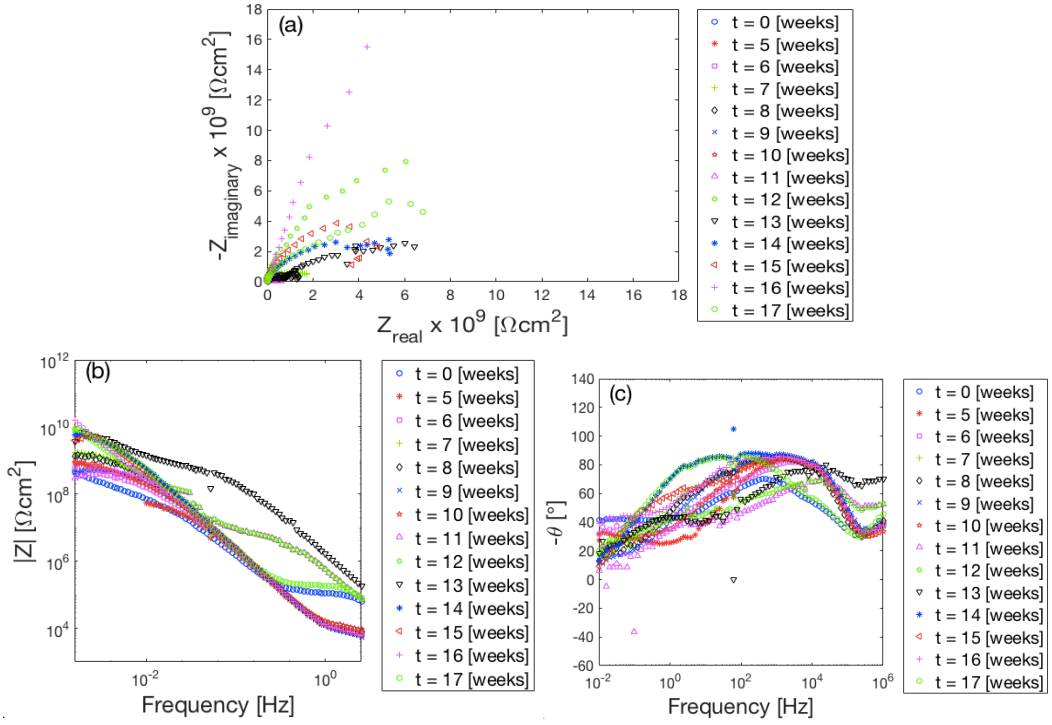

Figure A-2. Nyquist (a), Bode (b), and phase angle (c) plots for rebar in concrete with *w/c* of 0.45 at 3 cm deep under predominant wind.

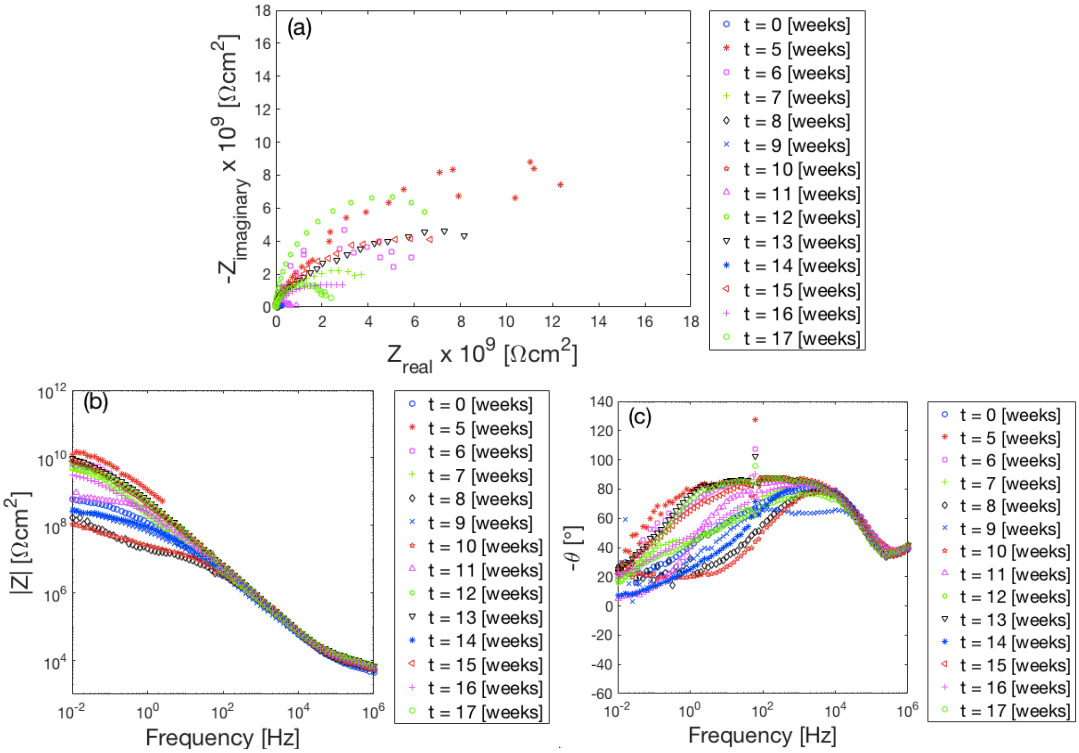

Figure A-3. Nyquist (a), Bode (b), and phase angle (c) plots for rebar in concrete with *w/c* of 0.65 at 1.5 cm deep under non-predominant wind.

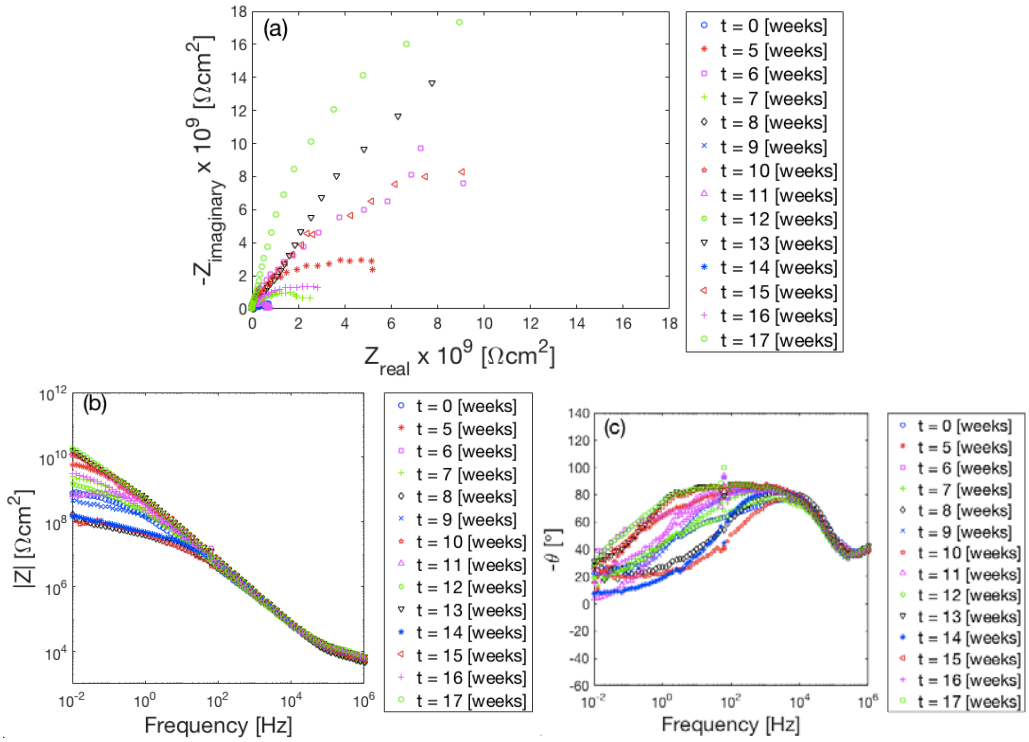

Figure A-4. Nyquist (a), Bode (b), and phase angle (c) plots for rebar in concrete with *w/c* of 0.65 at 1.5 cm deep under predominant wind.

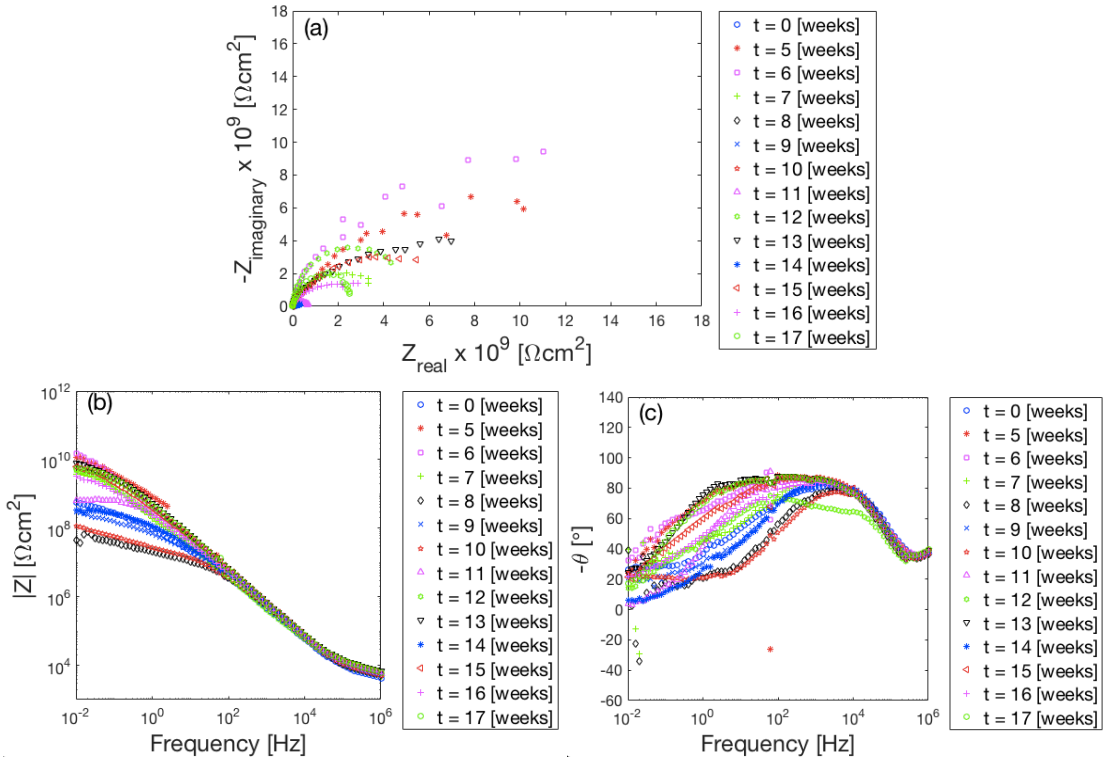

Figure A-5. Nyquist (a), Bode (b), and phase angle (c) plots for rebar in concrete with *w/c* of 0.65 at 2 cm deep under non-predominant wind.

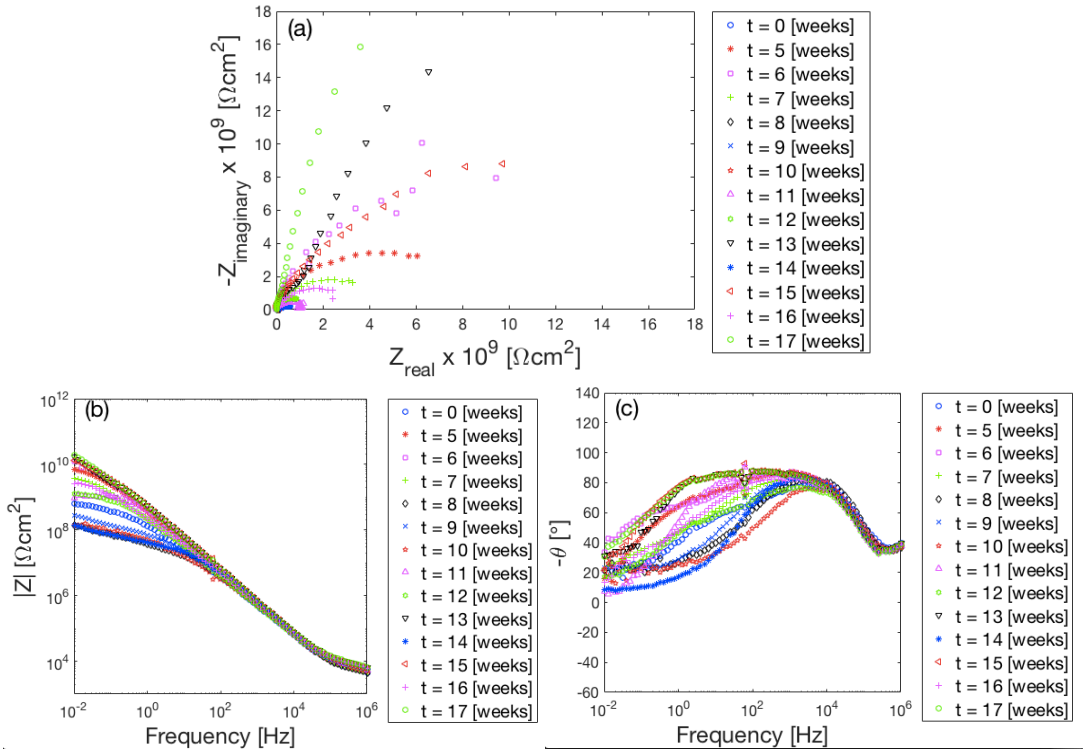

Figure A-6. Nyquist (a), Bode (b), and phase angle (c) plots for rebar in concrete with *w/c* of 0.65 at 2 cm deep under predominant wind.

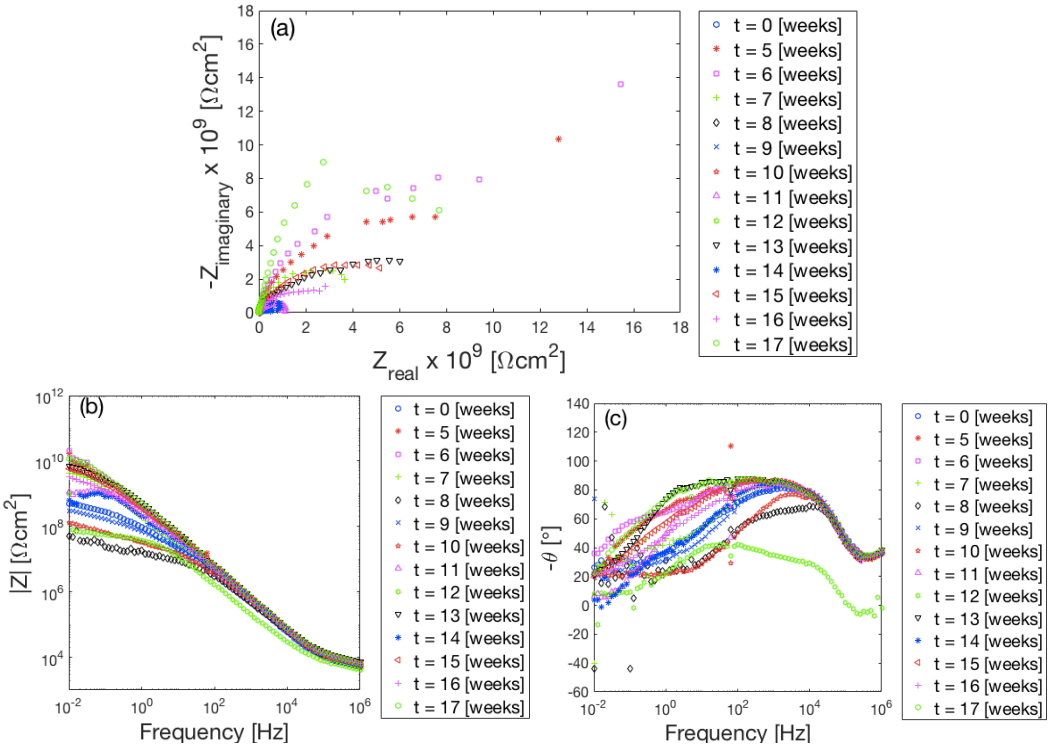

Figure A-7. Nyquist (a), Bode (b), and phase angle (c) plots for rebar in concrete with *w/c* of 0.65 at 3 cm deep under non-predominant wind.

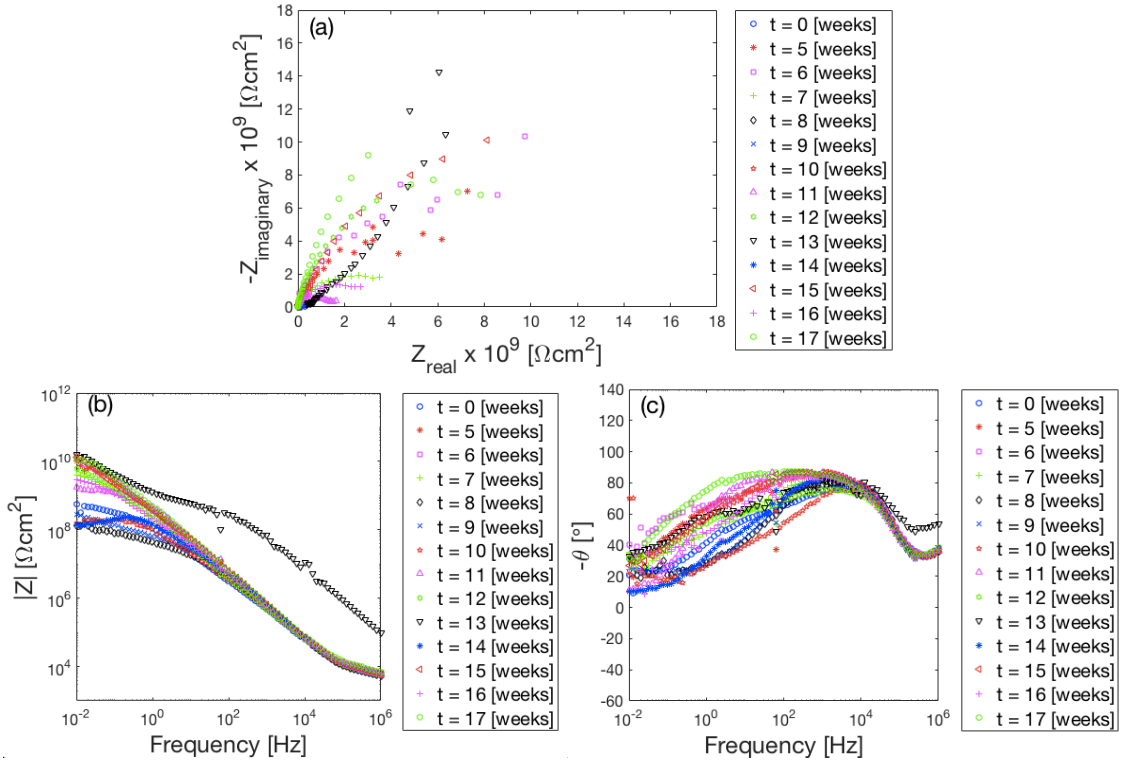

Figure A-8. Nyquist (a), Bode (b), and phase angle (c) plots for rebar in concrete with *w/c* of 0.65 at 3 cm deep under predominant wind.

APPENDIX B: SENSITIVITY ANALYSIS AND IMPORTANCE OF VARIABILITY

Figures B-1 to B-4 show the results of a basic sensitivity analysis. Figures B-1 and B-2 represent how the normalized sensitivity of each parameter changes over time. Through this analysis, it could be estimated that which parameter in the model can influence most on the model reliability. Such results may provide guidance for future studies regarding data gathering and model development. However, it is not proper to compare among the parameters, as they have different units.

Figure B-3 and B-4 show the change of importance measures for the parameters in the corrosion initiation estimation model. In both Figures, it was estimated that C_s, C_{cr}, d_c, and θ_3 are the parameters considered most important in the corrosion initiation time estimation.

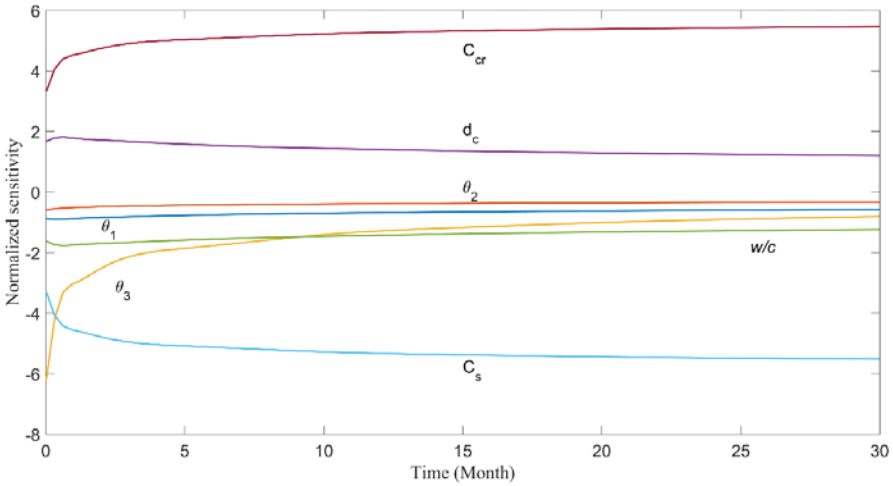

Figure B-1. Sensitivity analysis at *w/c* = 0.50 and surface concentration = 0.18.

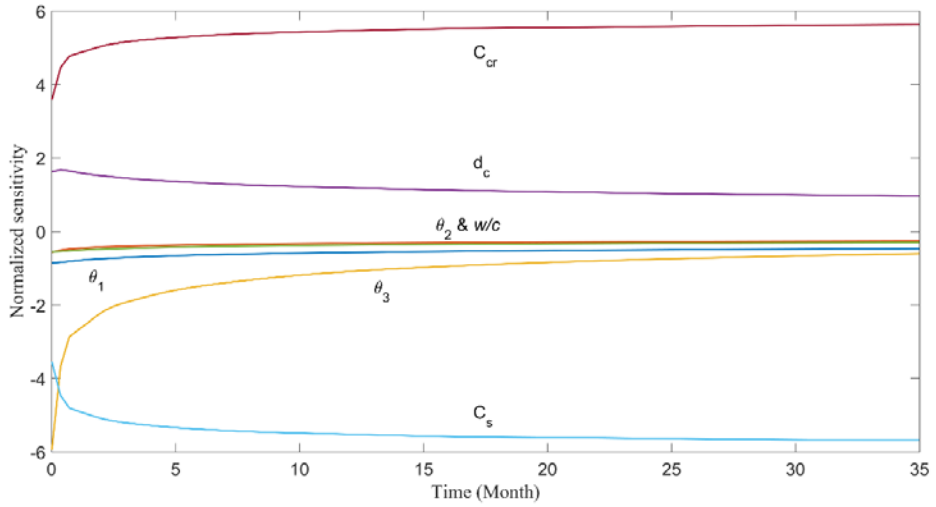

Figure B-2. Sensitivity analysis at *w/c* = 0.70 and surface concentration = 0.08.

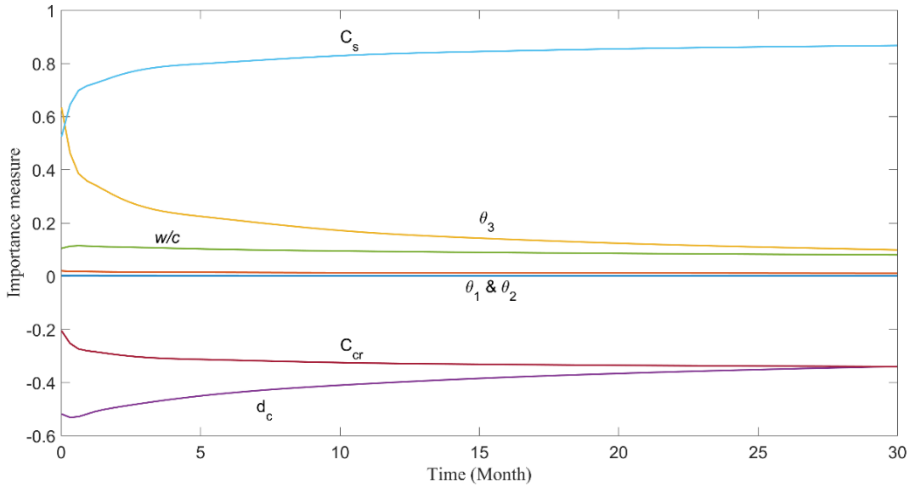

Figure B-3. Importance of variability at *w/c* = 0.50 and surface concentration = 0.18.

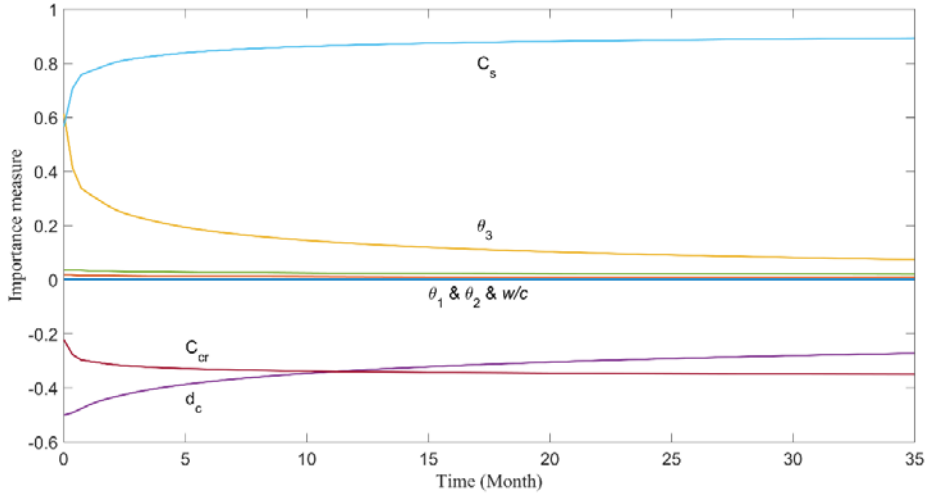

Figure B-4. Importance of variability at *w/c* = 0.70 and surface concentration = 0.08.